Journal of Organometallic Chemistry 892 (2019) 1–17

Contents lists available at ScienceDirect

Journal of Organometallic Chemistry

journal homepage: www.elsevier.com/locate/jorganchem

Homoleptic *cis*- and *trans*-palladium(II) bis(guanidinato) complexes derived from *N*-aryl-*N*′,*N*″-di(pyridin-2-yl)- and *N*-aryl-*N*′,*N*″-bis(6-methylpyridin-2-yl)guanidines: Catalysts for Heck-Mizoroki coupling reactions

Vishwesh Mishra [a], Jisha Mary Thomas [b], Sivasankar Chinnappan [b], Natesan Thirupathi [a, *]

[a] Department of Chemistry, University of Delhi, Delhi, 110 007, India
[b] Catalysis and Energy Laboratory, Department of Chemistry, Pondicherry University (A Central University), Puducherry, 605 014, India

ARTICLE INFO

Article history:
Received 21 December 2018
Received in revised form
20 March 2019
Accepted 10 April 2019
Available online 20 April 2019

Keywords:
Palladium
Guanidine
Homoleptic palladium(II) amido complex
Heck-Mizoroki coupling
Geometrical isomers

ABSTRACT

N-Aryl-*N*′,*N*″-di(pyridin-2-yl)- and *N*-aryl-*N*′,*N*″-bis(6-methylpyridin-2-yl)guanidines (**1**–**4** and **5**–**7**) were isolated in 75%–81% yields. Reactions of $Pd(OAc)_2$ with guanidines **2**–**7** carried out separately in toluene at 60 °C for 3 h afforded **8**–**13** respectively in 69%–80% yields. Compounds **1**–**13** were characterized by elemental analyses, HR-MS, IR and NMR (^1H and ^{13}C) spectroscopy. Molecular structures of guanidines **1**, **4**, **5** and **6** and those of **8**–**13** were determined by single crystal X-ray diffraction. The Pd(II) atom in **8**–**10** revealed *trans* geometry while that in **11**–**13** revealed *cis* geometry. DFT calculations were carried out on model compounds **9a** (*trans*) and its hypothetical *cis* isomer, **9b** and **12a** (*cis*) and its hypothetical *trans* isomer **12b** which indicated a very small energy difference between the **9a**/**9b** pair (1.28 kcal/mol) whereas a large energy difference was observed between the **12a**/**12b** pair (26.38 kcal/mol) in CH_2Cl_2. The catalytic utility of **9** in Heck-Mizoroki coupling reactions involving styrene and methyl acrylate and aryl bromides/aryl chlorides in the presence of NaOAc and excess of tetrabutylammonium bromide (TBAB) at 120 °C was explored. Both activated and de-activated aryl bromides and aryl chlorides were coupled with styrene and in addition, the aryl chlorides were coupled with methyl acrylate in the presence of **9** to afford the respective coupling products in 68% – >99% yields. Neat reaction carried out with **9** and TBAB under the optimized condition released the colloidal Pd black as verified by EDAX, PXRD and SEM techniques thereby implying the heterogeneous nature of catalysis.

1. Introduction

Transition metal complexes of *sym N*,*N*′,*N*″-trisubstituted guanidines, $(RNH)_2C=NR$ (*sym* = symmetrical; R = alkyl and aryl) are well known in the literature due to their intriguing structural aspects and reactivity pattern [1]. In these complexes, guanidines are present in neutral, monoanionic (i.e., guanidinate(1−)) and dianionic (i.e., guanidinate(2−)) forms and exhibit chelating and bridging coordination modes. Palladium(II) complexes of *sym N*,*N*′,*N*″-triphenylguanidine, $[(PhNH)_2C=NPh]$ are known wherein the guanidine is present in neutral and monoanionic forms [2,3]. *Sym N*,*N*′,*N*″-tris(2-hydroxybenzylidene)triaminoguanidine, LH_6Cl upon reaction with $(Et_4N)_2(PdCl_4)$ in MeCN in the presence of Et_4NOH afforded $(Et_4N)_2(LPd_3Cl_3)\cdot MeCN$ wherein the anion was shown to possess a chiral propeller-like conformation in solid state [4]. Palladium(II) complexes of *N*-substituted guanidines as well as six-membered palladacyclic complexes derived from guanidines were used as effective phosphine free catalysts in Heck and Suzuki cross coupling reactions [5–7]. *Trans*-$[PdCl_2\{(^iPrNH)_2C=NAr\}_2]$ were shown to be intermediates in guanylation reactions of 4-anisidine, 2-fluoro-4-iodoaniline and 3,4-(methylenedioxy)aniline by *N*,*N*′-diisopropylcarbodiimide catalyzed by Pd(II) source [8].

N-Substituted amidines and formamidines with additional *N*-donor sites and their metal complexes are known in the literature [1c] while metal complexes of *N*-substituted guanidines with additional *N*-donor sites remain unknown presently. We prepared *N*-substituted unsymmetrical guanidines **1**–**7** in order to understand whether this family of guanidines will undergo C–H or N–H

* Corresponding author.
E-mail addresses: thirupathi_n@yahoo.com, tnat@chemistry.du.ac.in (N. Thirupathi).

https://doi.org/10.1016/j.jorganchem.2019.04.009
0022-328X/

activation upon treatment with Pd(II) source. From this endeavor, interestingly, two types of geometrical isomers namely **8**–**10** (*trans*) and **11**–**13** (*cis*) were isolated via N–H activation of guanidines and these complexes were fully characterized. Molecular structures of four guanidines (**1**, **4**, **5** and **6**) and those of complexes **8**–**13** were determined by single crystal X-ray diffraction (SCXRD). The utility of **9** as a catalyst in Heck-Mizoroki coupling reaction (H-MCR) involving styrene and methyl acrylate and aryl bromides and aryl chlorides as coupling partners were explored.

2. Results and discussion

2.1. Syntheses

Reactions of *N*,*N*′-di(pyridin-2-yl)thiourea and *N*,*N*′-bis(6-methyl pyridin-2-yl)thiourea with variously substituted anilines in the presence of 70% aqs. KOH in nitrobenzene following the procedure previously reported by us on the preparation of *sym N*,*N*′,*N*″-triarylguanidines [9] afforded *N*-aryl-*N*′,*N*″-di(pyridin-2-yl) guanidines, **1**–**4** and *N*-aryl-*N*′,*N*″-bis(6-methylpyridin-2-yl)guanidines, **5**–**7** in 75%–81% yields as illustrated in Scheme 1. Guanidine **2** is known in the literature [10] but it was prepared from the reaction of *N*-(2-pyridyl)-*N*′-(4-tolyl)carbodiimide with 2-aminopyridine in 18% yield which is far inferior than our yield of 76% obtained through the route illustrated in Scheme 1.

Reactions of $Pd(OAc)_2$ with guanidines, **2**–**7** carried out separately in toluene at 60 °C for 3 h afforded **8**–**13** respectively in 69%–80% yields as illustrated in Schemes 2 and 3. A plausible mechanism of the formation of **8**–**13** is shown in Scheme 4. The reaction of $Pd(OAc)_2$ with the guanidine could afford a transient intermediate **A** due to chelate effect and this intermediate upon amine-imine tautomerisation could afford another intermediate **B**. Subsequently, the intermediate **B** upon N–H activation via the loss of AcOH could afford either a dinuclear intermediate **C** or a mononuclear intermediate **D** depending upon the steric encumbrance of the R group in the coordinated pyridyl or methyl pyridyl units of the guanidine. It is believed that sterically less hindered coordinated 2-pyridyl ring in the intermediate **C** stabilizes the dinuclear core, $[Pd(\mu_2\text{-}OAc)]_2$ while sterically more hindered 6-methyl-2-pyridyl ring in the intermediate **D** stabilizes the mononuclear core, $[Pd(\kappa^2\text{-}OAc)]$. Compounds of both types **C** and **D** are known in the literature and a few of these complexes are crystallographically characterized [11]. Our attempts to secure NMR experimental support for the aforementioned hypothesis were thwarted as reactions of $Pd(OAc)_2$ with **2** and **3** carried out separately in toluene even at ambient temperature lead to the precipitate formation in each case and these precipitates were subsequently isolated and identified as **8** and **9**, respectively.

2.2. X-ray crystallography

Molecular structures of guanidines **1** and **4**–**6** were determined by SCXRD and are shown in Figs. 1 and 2. In principle, *sym N*,*N*′,*N*″-triarylguanidines can exhibit four different conformations namely *syn-syn, syn-anti, anti-syn* and *anti-anti* [9]. From the dispositions of the aryl and the pyridyl substituents of amino N atoms with reference to the >C=N– unit in **1** and **4**–**6**, *syn-anti* conformation is evident in solid-state. In this conformer in all guanidines, there are two intramolecular N–H···N hydrogen bonds involving pyridyl N atom and H atom of the amino moiety and further in guanidines **1** and **4**, one intramolecular C–H···N hydrogen bond involving an imino N atom and *o*-hydrogen atom of the aryl ring is observed (see Fig. 1). The aforementioned intramolecular E–H···N (E = N and C) hydrogen bonds places all non-hydrogen atoms of pyridyl and aryl rings in a plane which almost coincides with the plane of the CN_3 unit of the guanidine. The angle between the mean plane of the CN_3 unit and the mean plane of the aryl and pyridyl rings attached to the N atom of the CN_3 unit respectively are 3.8(2)°, 6.9(1)° and 4.5(1)° (**1**), 3.2(5)°, 5.1(6)° and 5.4(6)° (**4**), 1.5(1)°, 9.6(1)° and 4.9(1)° (**5**) and 1.8(4)°, 4.2(4)° and 5.4(4)° (**6**). Both the amino N atoms and the carbon atom of the CN_3 unit in all guanidines are planar ($\Sigma \approx 360°$).

A somewhat planar disc shaped molecule of **1** are stacked one over the other in *anti*-parallel fashion continuously while a similar

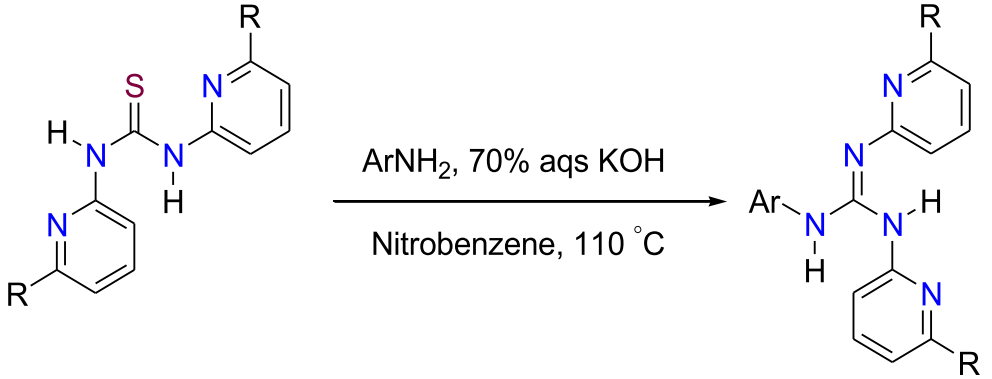

1–7

	Ar	R		Ar	R
1	2-MeC_6H_4	H	**5**	4-MeC_6H_4	Me
2	4-MeC_6H_4	H	**6**	4-ClC_6H_4	Me
3	4-ClC_6H_4	H	**7**	4-FC_6H_4	Me
4	4-BrC_6H_4	H			

Scheme 1. Synthesis of guanidines, **1**–**7**.

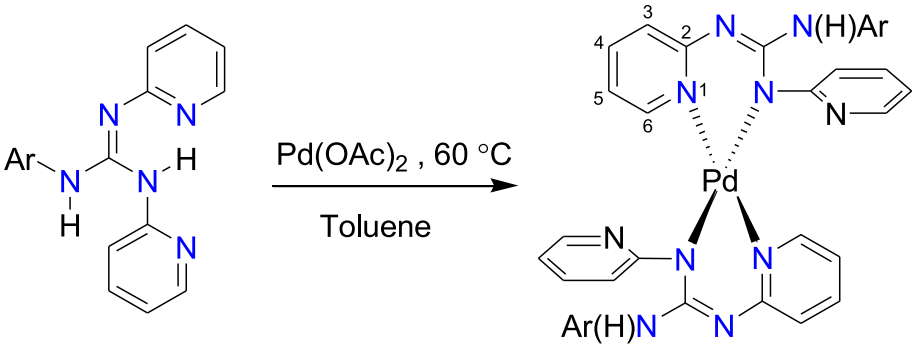

	Ar	
2	4-MeC_6H_4	**8**
3	4-ClC_6H_4	**9**
4	4-BrC_6H_4	**10**

Scheme 2. Synthesis of *trans* configured homoleptic palladium(II) bis(guanidinato) complexes, **8**–**10**.

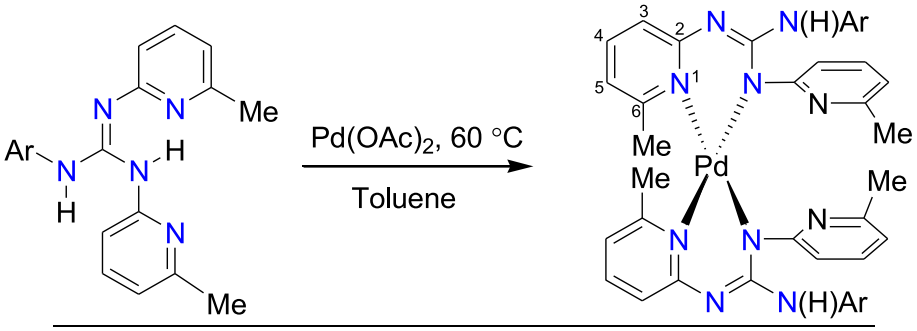

	Ar	
5	4-MeC_6H_4	**11**
6	4-ClC_6H_4	**12**
7	4-FC_6H_4	**13**

Scheme 3. Synthesis of *cis* configured homoleptic palladium(II) bis(guanidinato) complexes, **11**–**13**.

disc shaped molecules of **4** and **6** are stacked one over the other in parallel fashion continuously and this growth leads to the formation of a one-dimensional column (see the Supplementary data). The two one-dimensional columns are further linked through a weak intermolecular hydrogen bonds such as C–H···N, C–H···X (X = Cl and Br) and N–H···Br and the columns are stacked at an angle of 66.39° (**1**), 78.83° (**4**) and 73.89° (**6**) with each other. In the case of **5**, no such stacking arrangement is observed in the crystal lattice.

Molecular structures of **8**–**13** were determined by SCXRD and are shown in Figs. 3 and 4. Complexes **8**–**10** revealed *trans* geometry around the Pd(II) atom while complexes **11**–**13** revealed *cis* geometry. The angle between two mean planes constituted by N1Pd1N5 and N6Pd1N10 in **8** is 0.5(1)° and the corresponding angle in **9** and **10** are 0.0(1)° and 0.0(2)° respectively indicating a very minimal or no distortion around the Pd(II) atom in these complexes. However, the angle between two mean planes constituted by N1Pd1N5 and N6Pd1N10 in **11** is 10.2(1)° and the corresponding angle in **12** and **13** are 10.4(1)° and 12.2(1)° respectively indicating a significant distortion around the Pd(II) atom in these complexes.

Key structural parameters of **8**–**13** are listed in Table 1. The two six-membered rings linked by the Pd(II) atom in these complexes revealed a pseudo boat conformation. The Pd(II) atom deviates from the basal plane of the pseudo boat more than the imine N atom as reflected from the greater values of x and x' than those of y and y' and the greater values of θ_1 and θ_1' than those of θ_2 and θ_2'. Further, the magnitude of distortion around the Pd(II) atom is greater in **11**–**13** than in **8**–**10**. This difference arises due to both steric and electronic factors. The repulsive interaction between Me groups in two *cis* positioned coordinated 6-methyl 2-pyridyl substituent of the chelate rings in **11**–**13** causes more geometrical distortion around the Pd(II) atom. Further, both the amido N atoms in **8**–**10** and **11**–**13** can act as σ and π-donors to the Pd(II) atom. It has been shown for four-membered lithium amidinate complexes that the Li atom moves towards the plane of a charge delocalized

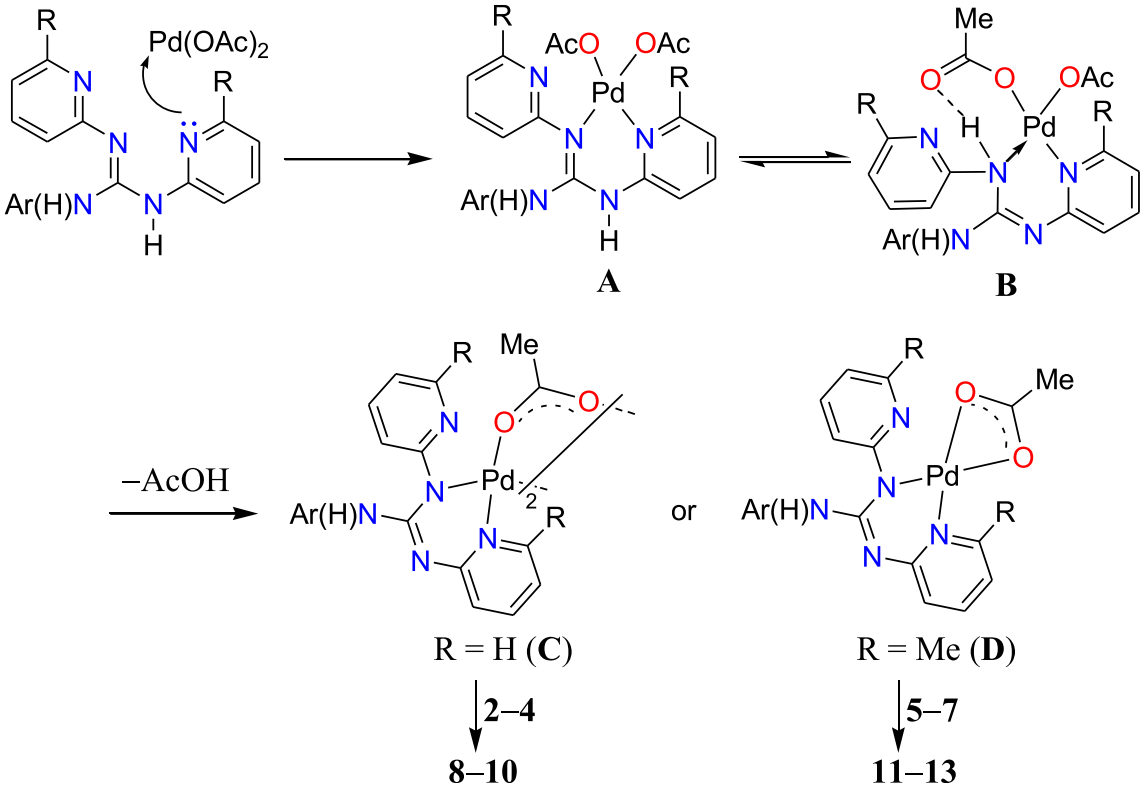

Scheme 4. Plausible mechanism of the formation of complexes **8**–**13**.

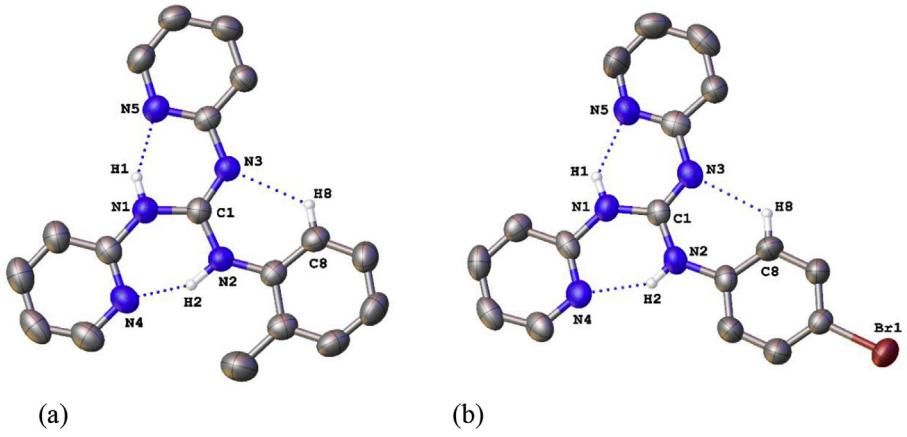

Fig. 1. Molecular structures of **1** (a) and **4** (b) at 50% probability level. Only hydrogen atoms involved in hydrogen bonding are shown for clarity.

diazally anion, $\{(Me_3Si)NC(R)N(SiMe_3)\}^-$ when the N atom in this anion acts as a σ-donor while the Li atom moves above the plane of the anion when the N atom acts as a π-donor [12]. The CN_3 carbon atom and the exocyclic amino N atom in **8**–**13** are planar while the amido N atom slightly deviates from planarity. Thus, the amido N atom in **8**–**13** acts as σ and π-donors and additionally, there is a greater geometrical distortion around the Pd(II) atom in **11**–**13** due to steric factor. Homoleptic palladium(II) amido complexes with a *trans* geometry around the Pd(II) atom is more prevalent than the analogous complexes with a *cis* geometry [13,14].

Interestingly, an intramolecular π···π stacking interaction was observed between 6-methyl-2-pyridyl rings attached to N1 and N6 in **11**–**13** (π···π = 3.589 Å (**11**), 3.579 Å (**12**) and 3.599 Å (**13**)) and two intermolecular π···π stacking interactions were observed, between the pair of 6-methyl-2-pyridyl rings attached to the N1 atom and its centrosymmetric neighbor and another such pair attached to the N6 atom (π···π = 3.670 Å/3.668 Å (**11**), 3.684 Å/3.657 Å (**12**) and 4.010 Å/3.625 Å (**13**)). These intra- and intermolecular π···π stacking interactions are well within the defined boundary of 3.8 Å [15] except in **13**. As a representative example, these stacking interactions are illustrated for **11** in Fig. 5. These π···π stacking interactions are believed to be partly responsible for stabilization of *cis* configuration of the Pd(II) atom in **11**–**13**. Neither intramolecular nor intermolecular π···π stacking interactions such as those mentioned above were observed in the crystal lattice of **8**–**10**.

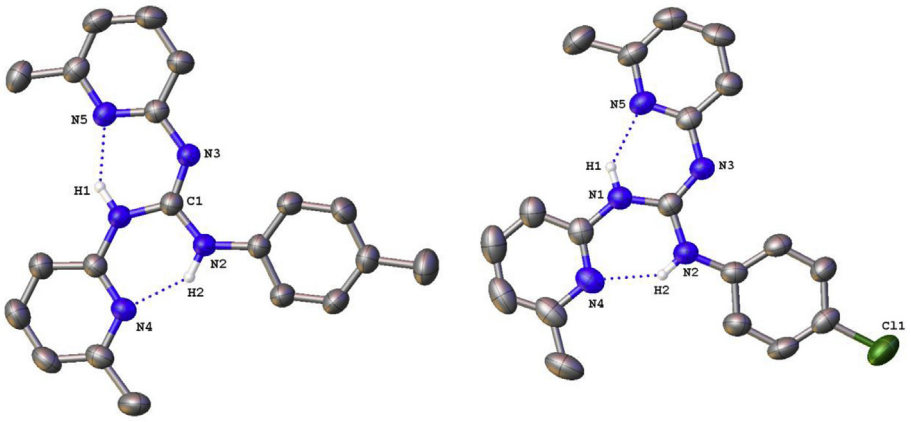

Fig. 2. Molecular structures of **5** (a) and **6** (b) at 50% probability level. Only hydrogen atoms involved in hydrogen bonding are shown for clarity.

2.3. DFT calculations

DFT calculations were performed on model compounds of **9** namely, **9a** (*trans*) and **9b** (*cis*) and model compounds of **12** namely, **12a** (*cis*) and **12b** (*trans*). All the four complexes were successfully optimized without any imaginary frequency and their optimized geometries are shown in Figs. 6 and 7. The energies of **9a**, **9b**, **12a** and **12b** in gas phase are listed in Table 2. A solvent correction for CH_2Cl_2 was performed using the polarized continuum model (PCM) on all the four complexes, the energies of which are also listed in Table 2. Selected bond parameters of **9a**, **9b**, **12a** and **12b** and the hydrogen bonding interactions in these complexes are listed in the Supplementary data.

Complex **9a** was found to be more stable than **9b** by a value of 1.28 kcal/mol, whereas complex **12a** was found to be more stable than **12b** by a value of 26.38 kcal/mol in CH_2Cl_2. It was noted that after optimization the geometry around the Pd(II) atom in **12b** changed drastically as seen from the bond angles around the Pd(II) atom (see the Supplementary data). *Cis*- and *trans*-NPdN angles between two chelate rings in **12b** are 96.79/96.77° and 143.83/157.05° instead of 90° and 180°, respectively. Thus, the optimized geometry contained a significant tetrahedral contribution for the Pd(II) atom in **12b**.

The optimized geometries of **9a** and **12a** are in complete agreement with the observed geometries of **9** and 12 respectively. The parameters *x*, *y*, θ_1 and θ_2 defined in Table 1 matched well with the corresponding values derived from DFT studies (see the Supplementary data). The values of *x*, *y*, θ_1, θ_1', θ_2 and θ_2' parameters for **9b** are similar to the corresponding values obtained for **9** and **9a**. Thus, we may conclude that **9** can possess either *cis* or *trans* geometries on the basis of energy and steric considerations but it prefers *trans* geometry in solid state due to packing forces. The Pd(II) atom in **12b** revealed a tetrahedrally distorted square planar environment as evident from the angle between two NPdN mean planes being 43.16°, quite larger than the ideal angle of 0.0°. Imposing a square planar geometry on the Pd(II) atom in **12b** would result in greater instability to the complex. Tetrahedrally distorted square planar geometry around the Pd(II) atom in $[PdN_4]^{2+}$ macrocyclic complex is reported in the literature [16]. Thus, it can be summarized that the formation of *trans* complexes **11**–**13** can be realized only when the environment around the Pd(II) atom is tetrahedrally distorted. Thus, steric factor predominantly dictates the *cis* configuration in **11**–**13**.

2.4. Heck-Mizoroki coupling reactions

H-MCR is one of the important C–C bond forming reactions [17]. Various Pd sources have been used as catalysts in H-MCR among which phosphine free palladium catalysts are the most attractive one from the commercial and toxicity points of view [5a,5b,7,14,17–19]. The Pd(II) amido complexes were shown to be one of the phosphine free catalysts used in H-MCR and this class of compounds are attractive as they are cheaper, stable to air and moisture and exhibit high activity [14,17c,18a]. Continuing our interests in utilizing Pd(II) complexes as phosphine free catalysts in cross coupling reactions [6,7], herein we report the utility of **8**–**13** and in particular the utility of **9** as catalyst in H-MCR involving styrene and aryl bromides or aryl chlorides and methyl acrylate and aryl chlorides as coupling partners.

Complexes **8**–**13** were screened for H-MCR involving styrene and 4-bromoanisole in the presence of NaOAc as the base, 0.1% catalyst and tetra-*n*-butyl ammonium bromide (TBAB) as a co-catalyst in the absence of solvent as illustrated in Scheme 5. The screening experiments based on two runs indicated the formation of the coupling product, *E*-1-(4′-methoxyphenyl)-2-phenylethene in 80%–98% yields as listed in Table 3. From the screening study and from the fact that **9** melts sharply at 259.47 °C without any decomposition while **12** decomposes at 308.27 °C, the former complex was chosen as the catalyst of choice for H-MCR involving other coupling partners (see DSC thermograms of **9** and **12** in the Supplementary data).

Ionic liquids have been used as a medium to carry out H-MCR [19]. TBAB melts at 105 °C and provides an ionic liquid medium. Moreover, its low cost and solubility in water simplifies the work up procedure [19]. A variety of bases have been used in Pd(II) catalyzed C–C bond forming reactions. In this study, eight bases were screened for the H-MCR illustrated in Scheme 5 and yields of the coupling product obtained with each base are listed in Table 4. The yields of coupling product varied from 90% to 98% calculated based on the average of two runs. Though NaOAc and $NaHCO_3$ afforded the coupling product in comparable yields, the former base was chosen for further catalytic studies. The progress of the reaction illustrated in Scheme 5 was monitored by TLC after every hour from the onset of the reaction and the reaction was complete only after 12 h.

H-MCR illustrated in Scheme 5 was carried out at 110 °C and 120 °C for 12 h. The progress of the reaction was monitored by TLC,

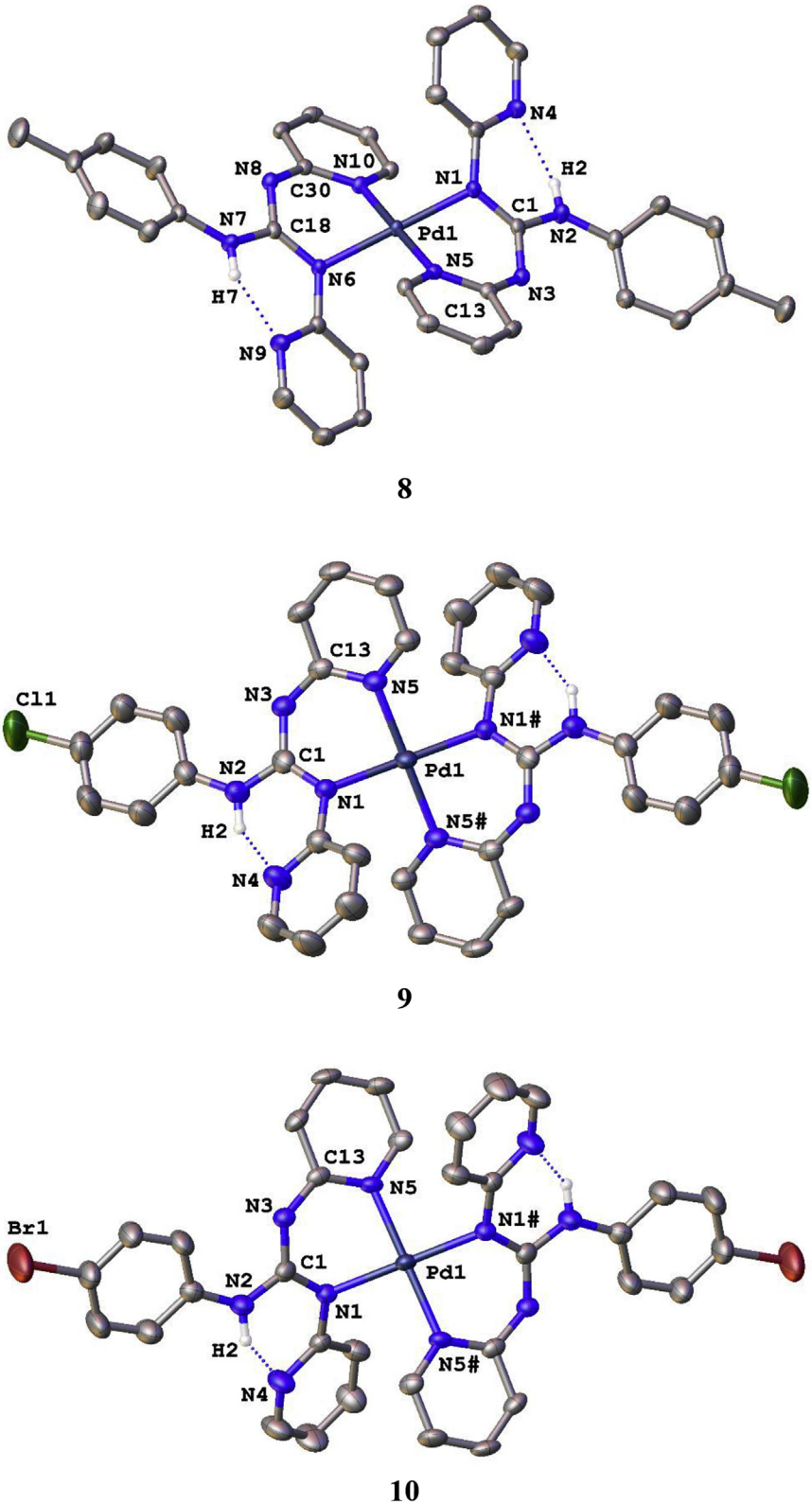

Fig. 3. Molecular structures of **8**, **9** and **10** at 50% probability level. Only hydrogen atoms involved in hydrogen bonding are shown for clarity.

which indicated the presence of both reactants and products when carried out at 110 °C while TLC of the reaction mixture carried out at 120 °C indicated complete consumption of 4-bromoanisole. A number of activated, deactivated and sterically hindered aryl bromides were coupled with styrene under optimized condition and from these reactions coupling products were isolated in ≥98% yields (Scheme 6 and Table 5).

The recyclability of the catalyst was studied up to five runs with

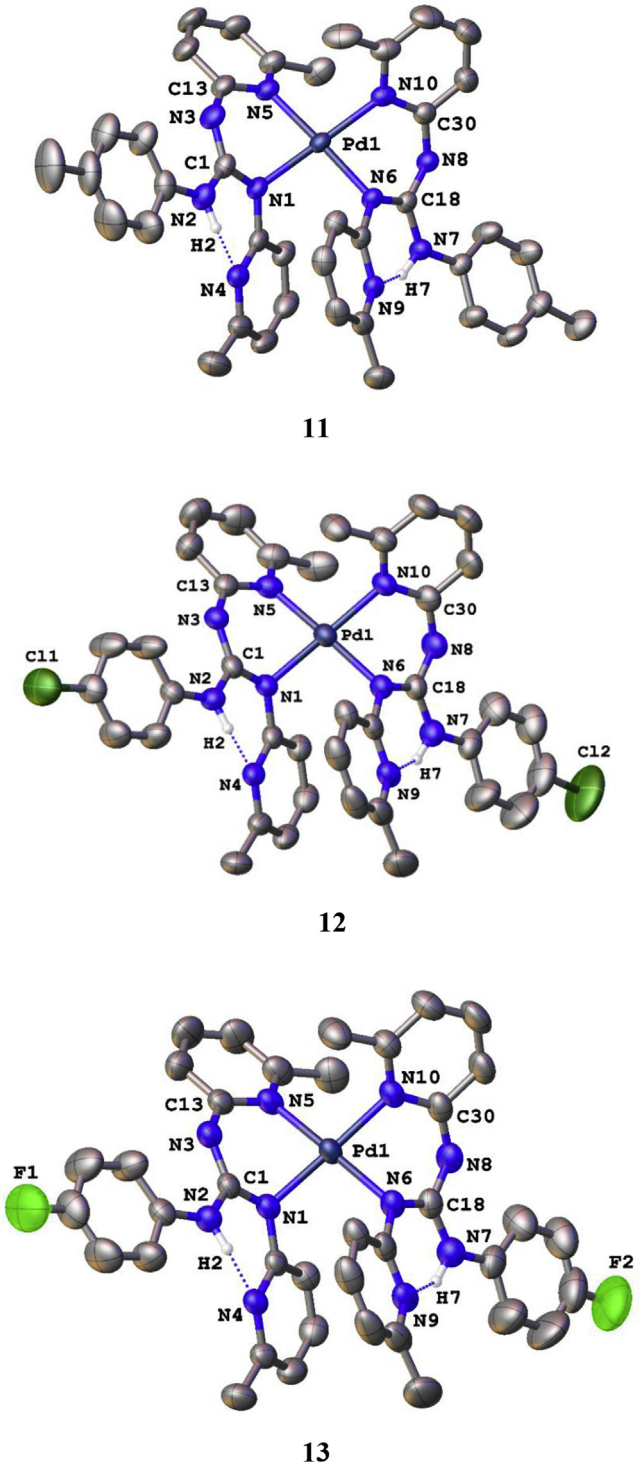

Fig. 4. Molecular structures of **11**, **12** and **13** at 50% probability level. Only hydrogen atoms involved in hydrogen bonding are shown for clarity.

styrene and 4-bromoanisole as coupling partner under the optimized condition by extracting the coupling product each time with diethyl ether and adding the coupling partners and base to the reaction mixture after each cycle. The yields of the coupling product in five consecutive cycles are 98%, 94%, 89%, 83% and 76%, respectively. The formation of Pd in various forms such as Pd colloids, Pd nanoparticles and anionic Pd complexes in H-MCR are well documented [18c,20]. The fact that we were able to reuse the residue after removal of the coupling product for further catalysis suggest that **9** releases colloidal Pd in situ and the latter catalyzes the reaction. The heterogeneous mixture consisting of **9** and TBAB were heated at 120 °C for 12 h to afford a dark reaction mixture which was subsequently diluted with chloroform and centrifuged to afford Pd black at the bottom. The Pd black was characterized by Energy Dispersive X-ray analysis (EDAX), powder X-ray diffraction (PXRD) and Scanning Electron Microscopy (SEM) (see Figs. 8–10). The PXRD pattern of Pd black exhibited five well defined characteristic Bragg's peaks appearing at $2\theta = 39.3°$, 45.92°, 67.72°, 81.46° and 86.14° which correspond to the (111), (200), (220), (311) and (222) crystal planes of face centered cubic structure of metallic Pd. For comparison, the standard pattern of Pd obtained from JCPDS (Card No. 46–1043) is also shown in Fig. 9. The SEM image illustrates that Pd black possesses a roughly spherical morphology with an average diameter of about 300 nm (see Fig. 10).

A comparative study of the catalytic efficacy of **9** in H-MCR of bromobenzene or 4-bromotoluene with styrene carried out in TBAB with those Pd(II) complexes in the related H-MCR in ionic liquid is summarized in Table 6 [5b,19c,19e]. Considering the catalyst loading, temperature and duration of the reaction, **9** appears to comparable or even better than those catalysts listed in Table 6.

H-MCR carried out separately with styrene and 4-bromopyridine and 2-bromopyridine under the optimized condition did not lead to the formation of coupling products suggesting the catalyst deactivation. Under the optimized condition, when $Pd(OAc)_2$ was used instead of **9** as a catalyst, styrene coupled with 4-bromoanisole to afford the coupling product in only 17% yield. This result illustrates beneficial effect of the guanidinato ligand environment around the Pd(II) atom in **9** in H-MCR.

Aryl chlorides are attractive substrates in cross coupling reactions as they are inexpensive. Nevertheless, aryl chlorides are relatively difficult to activate as the C–Cl bond is more inert than the C–Br bond in aryl bromides. The bond energies of C–X bonds in aryl halides mentioned above are 96 kcal/mol (X = Cl) and 81 kcal/mol (X = Br) [21]. When 4-chloroanisole was subjected to H-MCR with styrene under the optimized condition adopted for bromoarenes, the coupling product, *E*-1-(4′-methoxyphenyl)-2-phenylethene was isolated only in 52% yield. However, when the reaction was carried out in the presence of 0.5 mol% of **9**, the coupling product was isolated in 78% yield. Further, extending the reaction period up to 24 h improved the yield of the coupling product to 89%. Thus, the optimized reaction condition for H-MCR of aryl chlorides with styrene and methyl acrylate is illustrated in Scheme 7. Eight aryl chlorides were coupled with styrene under the optimized condition and from these reactions coupling products were isolated in 68%–95% yields (see Table 7). Both activated and deactivated aryl chlorides couple with styrene more efficiently than chlorobenzene (entries 1–3 and 4–7). Further, aryl chlorides were coupled with methyl acrylate under the condition illustrated in Scheme 7 and the coupling products were isolated in 85%–93% yields (see Table 8).

3. Conclusion

Guanidines **1**–**7** were prepared and isolated in good yields. Complexes **8**–**13** were prepared from $Pd(OAc)_2$ and guanidines, **2**–**7** through N-H activation. The new compounds were characterized by elemental analyses, mass spectrometry, IR and ^{1}H NMR spectroscopy. Molecular structures of **1** and **4**–**6** were determined by SCXRD which revealed *syn-anti* conformation in solid state. Molecular structures of **8**–**13** were also determined by SCXRD which revealed *trans* geometry (**8**–**10**) and *cis* geometry (**11**–**13**) around the Pd(II) atom. DFT calculations carried out on the **9a**/**9b** and the **12a**/**12b** pairs indicated a minimal energy difference

Table 1
Key structural parameters of **8**–**13**.

	8	9	10	11	12	13
x, x' (Å)	1.01(0), 0.96(0)	0.95(0)	0.96(0)	1.13(0), 1.14(0)	1.14(0), 1.15(0)	1.10(0), 1.14(0)
y, y' (Å)	0.20(0), 0.18(0)	0.19(0)	0.18(0)	0.24(0), 0.21(0)	0.21(2), 0.24(0)	0.22(0), 0.22(0)
θ_1, θ_1' (deg)	42.7(1), 40.5(1)	40.1(2)	40.4(4)	48.8(1), 49.1(1)	49.4(1), 49.1(1)	47.3(1), 49.0(1)
θ_2, θ_2' (deg)	19.0(3), 17.4(3)	18.3(4)	17.0(8)	21.9(1), 20.0(2)	19.2(2), 22.2(1)	20.5(3), 20.2(3)
ΣN_{amido} (deg)[a]	358.8, 357.1	358.3	358.2	355.5, 355.9	355.6, 355.4	355.9, 355.8

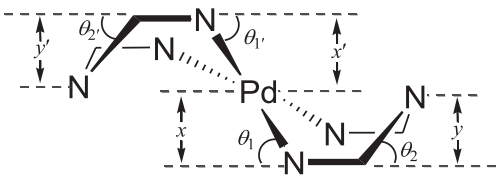

x and x' = distance of Pd(II) atom from the basal plane of the boat.
y and y' = distance of the imine N atom from the basal plane of the boat
θ_1 and θ_1' = angle between the basal plane of the boat and the plane defined by$(NPdN)_{ring\ 1}$/$(NPdN)_{ring\ 2}$.
θ_2 and θ_2' = angle between the basal plane of the boat and the plane defined by$(CN_{imine}C)_{ring\ 1}$/$(CN_{imine}C)_{ring\ 2}$.
[a] $\Sigma CN_3 \approx \Sigma N_{amino} \approx 360°$.

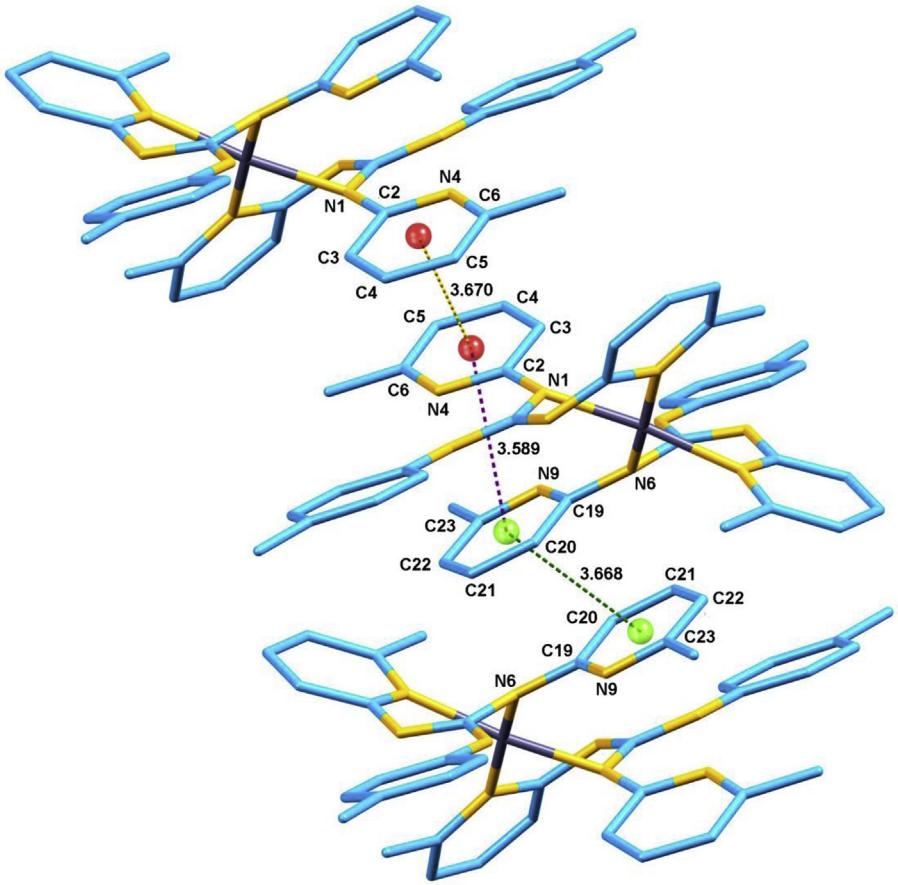

Fig. 5. Illustration of intra- and intermolecular $\pi\cdots\pi$ stacking interactions in **11**. The sphere inside the rings represent the centroid of the respective ring. The distances involving stacking interactions are given in Å.

(1.28 kcal/mol) and maximal difference, (26.38 kcal/mol), respectively. *Cis* geometry of the Pd(II) atom in **11**–**13** is shown to be dictated predominantly by the steric factor. Complex **9** was shown to be an excellent catalyst for H-MCR involving styrene and aryl bromides at 0.1 mol% catalyst loading and as a good catalyst for H-MCR involving styrene and methyl acrylate and aryl chlorides at 0.5 mol% catalyst loading. Neat reaction carried out with **9** and TBAB indicates that the former acts as a reservoir of colloidal Pd black in H-MCR as independently verified by EDAX, PXRD and SEM investigations and thus points out heterogeneous nature of catalysis.

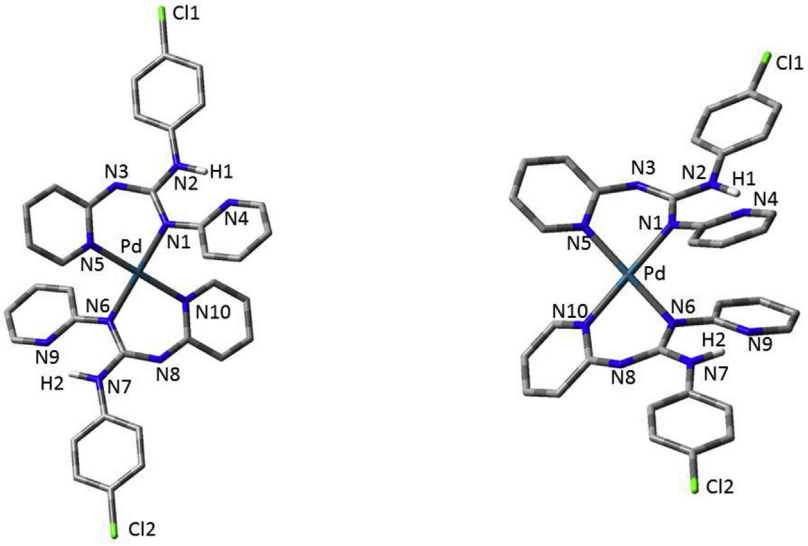

Fig. 6. Optimized structures of **9a** (a) and **9b** (b) isomers. All the hydrogen atoms except the one showing hydrogen bonding have been deleted for the sake of clarity.

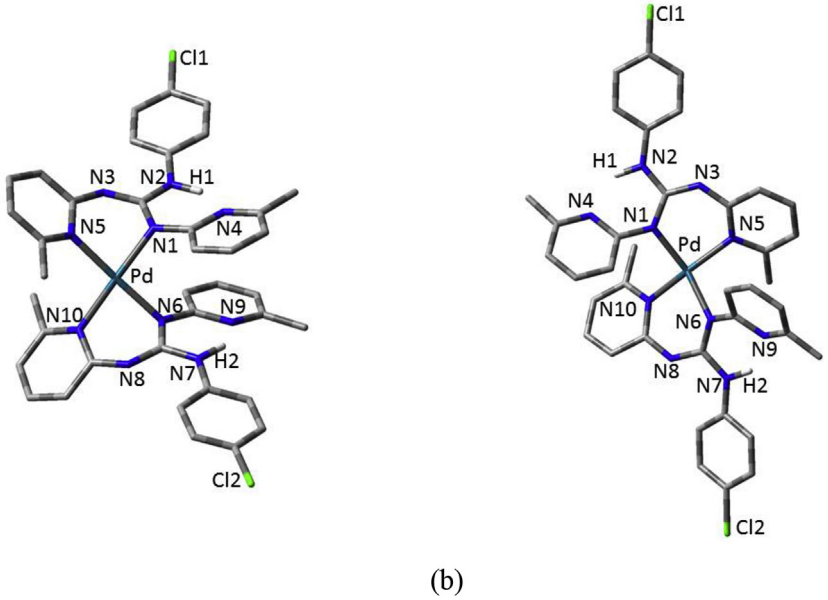

Fig. 7. Optimized structures of **12a** (a) and **12b** (b) isomers. All the hydrogen atoms except the one showing hydrogen bonding have been deleted for the sake of clarity.

Table 2
Absolute energies of **9a**, **9b**, **12a** and **12b** in gas phase and in solution phase (CH_2Cl_2).

	E (gas phase, Hartree)	E (CH_2Cl_2, Hartree)
9a	−2904.3695947	−2904.3828561
9b	−2904.3671082	−2904.3808183
12a	−3061.3088942	−3061.3222518
12b	−3061.267535	−3061.2802081

4. Experimental section

4.1. Materials and instrumentation

$Pd(OAc)_2$, anilines, NaOAc, styrene, methyl acrylate, aryl chlorides and aryl bromides (Sigma Aldrich), 2-aminopyridine and 2-amino-6-methylpyridine, CS_2, Et_3N, TBAB and Et_2O (Spectrochem) were purchased from commercial vendors and used as received. *N*,*N*′-di(pyridin-2-yl)thiourea and *N*,*N*′-bis(6-methyl pyridin-2-yl)thiourea were prepared following the literature procedure [22]. The IR spectral data were obtained through ATR method from powdered samples on an IRAffinity-1 Shimadzu FTIR spectrometer in the frequency range 400–4000 cm^{-1}. Elemental analyses were performed on an Elementar Analysensysteme GmbH VarioEL Cube. Time of flight mass (TOF–MS) spectra were recorded on Agilent Technologies 6530, Accurate-Mass Q-TOF LC/MS instrument using electrospray positive ion mode. ^1H NMR, $^{13}C\{^1H\}$ NMR and ^{19}F NMR spectra were recorded on a JEOL ECX 400 NMR spectrometer operating at 400, 100.5, and 376.5 MHz (with

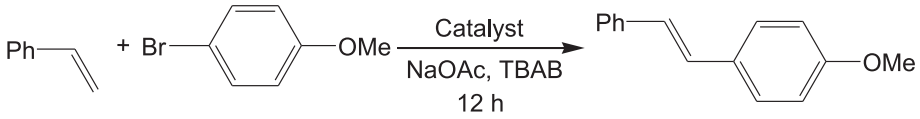

Scheme 5. Screening of complexes **8**–**13** as catalysts in the H−MCR of styrene and 4-bromoanisole. Styrene/4-bromoanisole/catalyst/NaOAc = 1.4/1.0/0.001/1.1 (mol).

Table 3
Results of screening of the complexes **8**–**13** as catalysts in the H−MCR of styrene and 4-bromoanisole.

Catalyst	Yield (%)	Catalyst	Yield (%)
8	92	**11**	81
9	98	**12**	87
10	93	**13**	80

The yield of the coupling product represents the isolated yield based on the average of two runs.

Table 4
Results of screening of the bases in the H−MCR of styrene and 4-bromoanisole.

Base	Yield (%)	Base	Yield (%)
NaOAc	98	K_2CO_3	94
$NaHCO_3$	98	Cs_2CO_3	95
Na_2CO_3	93	HCOONa	97
$KHCO_3$	95	K_3PO_4	90

The yield of the coupling product represents the isolated yield based on the average of two runs.

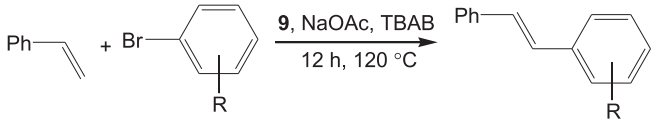

Scheme 6. Optimized reaction condition of H-MCRs of styrene and aryl bromides, ArBr. Styrene/ArBr/**9**/NaOAc = 1.4/1.0/0.001/1.1 (mol).

CF_3COOH as an external standard), respectively. The chemical shifts are reported in ppm relative to tetramethylsilane or residual solvent signal. Melting points were recorded on a Buchi melting point apparatus (Model: M−560) and the reported values are uncorrected.

SCXRD data for **1**, **4**–**6** and **8**–**13** were collected on Oxford Xcalibur S diffractometer (4-circle kappa goniometer, Sapphire−3 CCD detector, omega scans, graphite monochromator, and a single wavelength Enhance X-ray source with MoKα radiation) [23]. Pre-experiment, data collection, data reduction, and absorption corrections were performed with the CrysAlisPro software suite [24]. The structures were solved and refined using the SHELX-2017 program package [25] and SHELXL-2017/1 (within the WinGX program package) [26]. Non-hydrogen atoms were refined anisotropically. C−H/N−H hydrogen atoms were placed in geometrically calculated positions by using a riding model (except those in **1** and **4**–**6** which have been located from difference Fourier map) and refined. The molecular structures were created with Olex2 program [27]. Details of data collection, structure solution, refinement, selected bond parameters and packing diagrams for **1**, **4**–**6** and **8**–**13** are presented in Supplementary data.

SEM and EDAX analyses were carried out on a JEOL JSM-6610LV scanning electron microscope equipped with EDS. PXRD was carried out using a Rigaku Ultima (IV) diffractometer with Cu−Kα radiation at a scanning rate of 2° min^{-1} in the 2θ range of 30–90° (40 kV, 40 mA).

DFT calculations were performed on **9a**, **9b**, **12a**, and **12b** using the density functional theory (B3LYP) [28–30]. Cl, N, C and H atoms were described using the 6-31G* basis set [31] and the Pd atom was described using the LANL2DZ basis set [32–35]. The solvent correction for CH_2Cl_2 was carried out using the PCM [36–38]. The computational analyses on **9a**, **9b**, **12a** and **12b** were carried out using the Gaussian 09 software [39].

4.2. *[RN=C(NHR)(NHAr)] (R = 2-C_5H_4N, Ar = 2-MeC_6H_4; **1**)*

N,N′-Di(pyridin-2-yl)thiourea (230 mg, 1.00 mmol), 2-toluidine (118 mg, 1.10 mmol), KOH (140 mg as 70% aq. solution) and nitrobenzene (100 mg) were charged into a 25 mL round bottom (RB) flask. The contents in the RB flask were gradually heated up to 110 °C and maintained at the same temperature, while being stirred for 8 h. The reaction mixture was cooled to room temperature and diluted with water (10 mL). The organic portion was extracted with CH_2Cl_2 (3 × 5 mL) and the extract dried over anhydrous Na_2SO_4 for an hour and filtered. The volatiles from the filtrate were removed under vacuum to afford a yellow solid. The yellow solid was dispersed in *n*-hexane (10 mL), stirred for 15 min and allowed to stand. The soluble portion was discarded. This process was repeated two more times to afford a white solid. The solid was filtered off and washed with diethyl ether (2 × 10 mL), and dried on a hot plate at 70 °C for 6 h to afford the guanidine **1**. Yield: 81% (246 mg, 0.81 mmol). Mp: 131 °C. ATR−IR (cm^{-1}): ν (NH) 2958 (s, m), 2926 (s, m); ν (C=N) 1569 (s, sh). ^{1}H NMR ($CDCl_3$, 400 MHz): δ 2.45 (s, 3 H, CH_3), 6.80 (br t, J_{HH} = 5.2 Hz, 1 H, Ar*H*), 6.89 (br t, J_{HH} = 5.2 Hz, 2 H, Ar*H*), 6.98–7.04 (m, 2 H, Ar*H*), 7.19–7.26 (m, 2 H, Ar*H*), 7.54 (t, J_{HH} = 7.0 Hz, 1 H, Ar*H*), 7.63 (t, J_{HH} = 6.8 Hz, 1 H, Ar*H*), 8.21 (dd, J_{HH} = 5.2; 1.6 Hz, 2 H, Ar*H*), 8.52 (br, 1 H, Ar*H*), 11.86 and 14.04 (each s, 2 × 1 H, N*H*). ^{13}C{^{1}H} NMR ($CDCl_3$, 100.5 MHz): δ 19.0 (CH_3), 113.3, 115.9, 116.8, 121.7, 122.7, 122.9, 126.3, 128.6, 130.2, 137.6, 138.2, 138.4, 145.1, 145.9, 149.2, 153.6 (ArCH/Ar*C*), 161.9 (CN_3). ESI Mass (HRMS) $[M+H]^+$ Calc. 304.1562, Found 304.1559.

4.3. *[RN=C(NHR)(NHAr)] (R = 2-C_5H_4N, Ar = 4-MeC_6H_4; **2**)*

Guanidine, **2** was prepared from *N,N′*-di(pyridin-2-yl)thiourea (230 mg, 1.00 mmol), 4-toluidine (118 mg, 1.10 mmol), KOH (140 mg as 70% aq. solution) and nitrobenzene (100 mg) by following the procedure analogous to that outlined for **1**. Yield: 76% (260 mg, 0.76 mmol). Mp: 107 °C. ATR−IR (cm^{-1}): ν (NH) 3026 (br, w); ν (C=N) 1653 (s, m). The ^{1}H NMR spectrum of **2** revealed the presence of two isomers in *ca* 1.00:0.05 ratio as estimated from the integrals of N*H* protons (see Fig. 11). ^{1}H NMR ($CDCl_3$, 400 MHz): δ 2.30 (s, 3 H, CH_3, Isomer 2), 2.35 (s, 3 H, CH_3, Isomer 1), 6.79 (t, J_{HH} = 6.0 Hz, 2 × 1 H, Ar*H*, Isomers 1 & 2), 6.89 (t, J_{HH} = 6.0 Hz, 2 H, Ar*H*, Isomer 1), 7.05 (d, J_{HH} = 8.0 Hz, 2 × 1 H, Ar*H*, Isomers 1 & 2), 7.16 (d, J_{HH} = 8.8 Hz, 2 × 2 H, Ar*H*, Isomers 1 & 2), 7.36 (t, J_{HH} = 8.0 Hz, 2 H, Ar*H*, Isomer 2), 7.55 (t, J_{HH} = 7.0 Hz, 2 × 1 H, Ar*H*, Isomers 1 & 2), 7.62 (t, J_{HH} = 7.2 Hz, 2 × 1 H, Ar*H*, Isomers 1 & 2), 7.73 (d, J_{HH} = 8.0 Hz, 2 H, Ar*H*, Isomer 1), 7.87 (d, J_{HH} = 7.2 Hz, 2 H, Ar*H*, Isomer 2), 8.23 (d, J_{HH} = 7.2 Hz, 2 H, Ar*H*, Isomer 1), 8.37 (d, J_{HH} = 2.8 Hz, 2 H, Ar*H*, Isomer 2), 11.95 (s, 1 H, NH, Isomer 1), 12.07 (s, 1 H, NH, Isomer 2), 13.96 (s, 1 H, NH, Isomer 1). The signal for second NH proton of isomer 2 was not observed. ^{13}C{^{1}H} NMR ($CDCl_3$, 100.5 MHz): δ 20.9 (CH_3), 113.3, 115.8, 116.8, 121.3, 121.6, 129.2, 132.2, 137.0, 137.5, 138.3, 145.1, 146.0, 149.0, 153.7 (ArCH/Ar*C*), 162.0 (CN_3). ESI Mass (HRMS) $[M+H]^+$ Calc. 304.1562, Found

Table 5
Details pertinent to H–MCRs involving styrene and various aryl bromides (see Scheme 6). The reported yield represents isolated yield based on an average of two runs.

Entry	Substrate	Product	Yield (%)
1	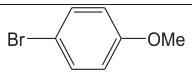	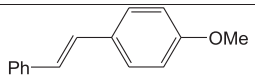	>99
2	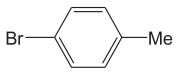	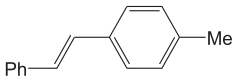	>99
3	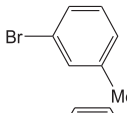	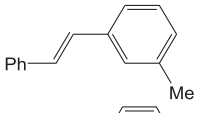	>99
4	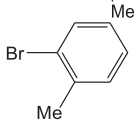	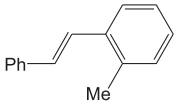	98
5	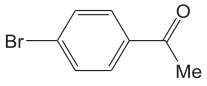	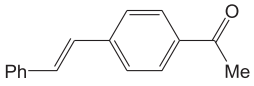	>99
6	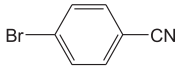	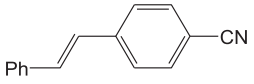	99
7	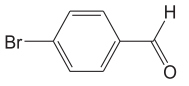	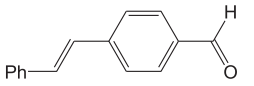	99
8	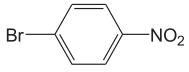	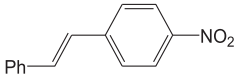	>99
9	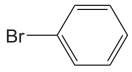	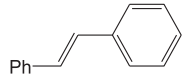	99

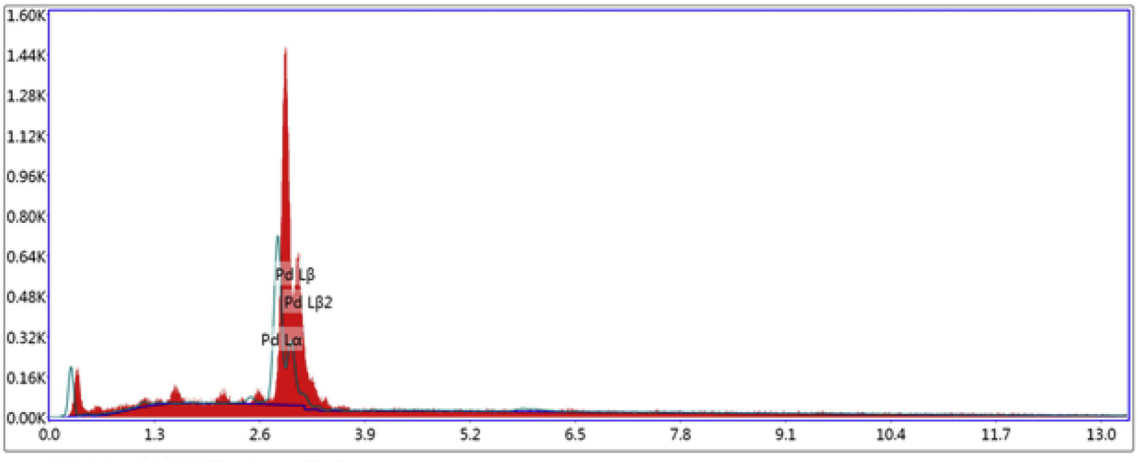

Fig. 8. EDAX graph for colloidal Pd obtained from neat reaction involving **9** and TBAB.

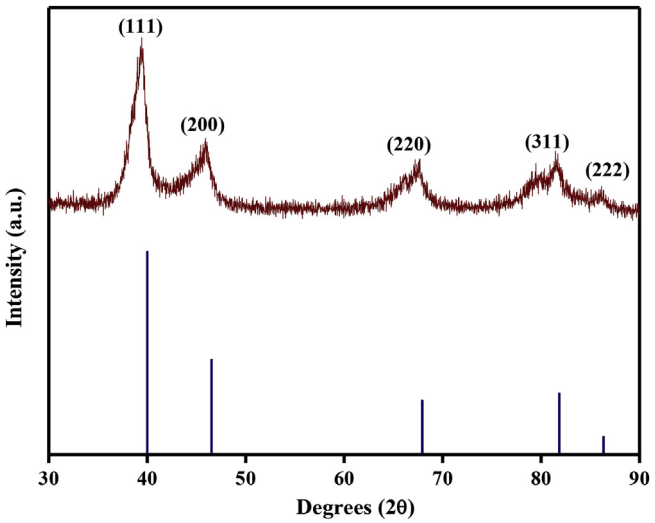

Fig. 9. Wide angle PXRD pattern obtained for colloidal Pd (top) obtained from neat reaction involving **9** and TBAB compared with the standard pattern of Pd obtained from JCPDS (Card No. 46–1043; bottom).

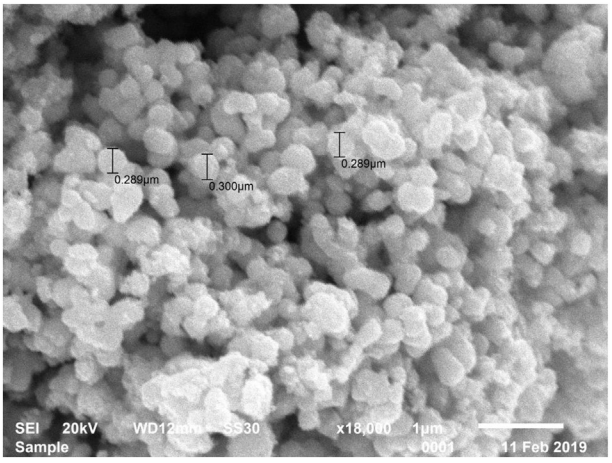

Fig. 10. SEM image of colloidal Pd obtained from neat reaction involving **9** and TBAB.

304.1551. Anal. Calc for $C_{18}H_{17}N_5$ (Mw = 303.361): C, 71.27; H, 5.65; N, 23.09. Found: C, 71.18; H, 5.36; N, 22.87.

4.4. *[RN=C(NHR)(NHAr)] (R = 2-C_5H_4N, Ar = 4-ClC_6H_4; **3**)*

Guanidine **3** was prepared from *N,N′*-Di(pyridin-2-yl)thiourea (230 mg, 1.00 mmol), 4-chloroaniline (140 mg, 1.10 mmol), KOH (140 mg as 70% aq. solution) and nitrobenzene (100 mg) by following the procedure analogous to that outlined for **1**. Yield: 78% (253 mg, 0.78 mmol). Mp: 137 °C. ATR–IR (cm^{-1}): *ν* (NH) 2999 (br, w); *ν* (C=N) 1649 (s, m). ^{1}H NMR ($CDCl_3$, 400 MHz): *δ* 6.82–6.90 (m, 3 H, Ar*H*), 7.05 (d, J_{HH} = 7.6 Hz, 1 H, Ar*H*), 7.29 (d, J_{HH} = 8.4 Hz, 2 H, Ar*H*), 7.57 (t, J_{HH} = 6.8 Hz, 1 H, Ar*H*), 7.63 (t, J_{HH} = 7.2 Hz, 1 H, Ar*H*), 7.82 (d, J_{HH} = 8.8 Hz, 2 H, Ar*H*), 8.23 (br, 2 H, Ar*H*), 12.13 and 13.98 (each, 2 × 1 H, N*H*). ^{13}C{^{1}H} NMR ($CDCl_3$, 100.5 MHz): *δ* 113.4, 116.2, 117.0, 121.6, 122.2, 127.3, 128.6, 128.7, 137.7, 136.3, 138.4, 145.1, 146.0, 148.7, 153.5 (Ar*C*H/Ar*C*), 161.6 (*C*N$_3$). ESI Mass (HRMS) $[M+H]^+$ Calc. 324.1016, Found 324.1007. Anal. Calc for $C_{17}H_{14}N_5Cl$ (Mw = 323.78): C, 63.06; H, 4.36; N, 21.63. Found: C, 63.37; H, 4.38; N, 22.00.

4.5. *[RN=C(NHR)(NHAr)] (R = 2-C_5H_4N, Ar = 4-BrC_6H_4; **4**)*

Guanidine **4** was prepared from *N,N′*-di(pyridin-2-yl)thiourea (230 mg, 1.00 mmol), 4-bromoaniline (189 mg, 1.10 mmol), KOH (140 mg as 70% aq. solution) and nitrobenzene (100 mg) by following the procedure analogous to that outlined for **1**. Yield: 75% (276 mg, 0.75 mmol). Mp: 171 °C. ATR–IR (cm^{-1}): *ν* (NH) 3015 (br, w); *ν* (C=N) 1655 (m). ^{1}H NMR ($CDCl_3$, 400 MHz): *δ* 6.81–6.87 (m, 2 H, Ar*H*) 6.91 (t, J_{HH} = 6.2 Hz, 1 H, Ar*H*), 7.06 (d, J_{HH} = 8.4 Hz, 1 H, Ar*H*), 7.43 (d, J_{HH} = 9.2 Hz, 2 H, Ar*H*), 7.58 (t, J_{HH} = 7.6 Hz, 1 H, Ar*H*), 7.64 (t, J_{HH} = 7.2 Hz, 1 H, Ar*H*), 7.78 (d, J_{HH} = 9.2 Hz, 2 H, Ar*H*), 8.23 (t, J_{HH} = 5.8 Hz, 2 H, Ar*H*), 12.13 and 13.98 (each, 2 × 1 H, N*H*). ^{13}C{^{1}H} NMR ($CDCl_3$, 100.5 MHz): *δ* 113.4, 114.9, 116.2, 117.0, 121.6, 122.6, 131.5, 137.7, 138.5, 138.8, 145.1, 146.0, 148.7, 153.5 (Ar*C*H/Ar*C*), 161.6 (*C*N$_3$). ESI Mass (HRMS) $[M+H]^+$ Calc. 368.0510, Found 368.0508. Anal. Calc for $C_{17}H_{14}N_5Br$ (Mw = 368.231): C, 55.45; H, 3.83; N, 19.02. Found: C, 55.64; H, 3.74; N, 19.05.

4.6. *[RN=C(NHR)(NHAr)] (R = 6-Me-2-C_5H_3N, Ar = 4-MeC_6H_4; **5**)*

Guanidine **5** was prepared from *N,N′*-bis(6-methyl pyridin-2-yl) thiourea (258 mg, 1.00 mmol), 4-toluidine (118 mg, 1.10 mmol),

Table 6
A comparative study of the catalytic efficacy of **9** with the previously reported catalysts in H-MCR carried out in ionic liquid.

Catalyst	Catalyst (mol)	Temp. (°C)	Time (h)	Yield (%)	Ref.
$PdCl_2$/GIL2	0.002	140	1.0	96[a]	5b
$Pd(OAc)_2$/Task specific ionic liquid	0.01	100	6.0	99[b]	19c
Bis(oxamato)palladate(II) complex/TBAB	0.005	120	4.0	92[b]	19e

[a] Styrene and 4-bromotoluene as coupling partner.
[b] Styrene and bromobenzene as coupling partner.

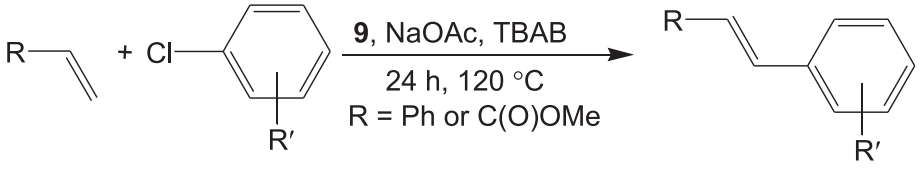

Scheme 7. Optimized reaction condition for the H–MCR of styrene or methyl acrylate and aryl chlorides, ArCl. Olefin/ArCl/**9**/NaOAc = 1.4/1.0/0.05/1.1 (mol).

Table 7
Details pertinent to H–MCR involving styrene and various aryl chlorides (see Scheme 7). The reported yield represents isolated yield based on an average of two runs.

Entry	Substrate	Product	Yield (%)
1	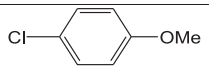	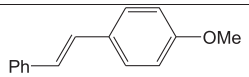	89
2	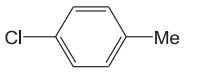	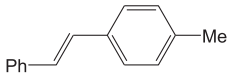	87
3	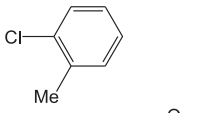	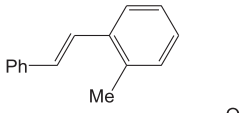	71
4	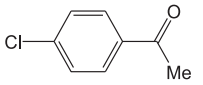	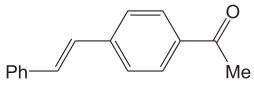	93
5	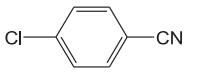	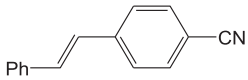	89
6	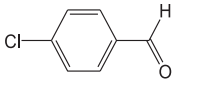	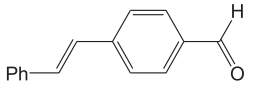	92
7	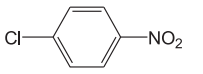	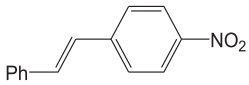	95
8		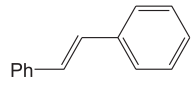	68

KOH (140 mg as 70% aq. solution) and nitrobenzene (100 mg) by following the procedure analogous to that outlined for **1**. Yield: 77% (255 mg, 0.77 mmol). Mp: 135 °C. ATR–IR (cm^{-1}): ν(NH) 2918 (br, w); ν (C=N) 1655 (m). The ^{1}H NMR spectrum of **5** revealed the presence of two isomers in *ca* 1.00:0.06 ratio as estimated from the integrals of N*H* protons (see Fig. 11). ^{1}H NMR ($CDCl_3$, 400 MHz): δ 2.34 (s, 3 H, CH_3, Isomer 1), 2.38 (s, 3 H, CH_3, Isomer 2), 2.52, 2.54 (each s, 2 × 3 H, CH_3, Isomer 1), 2.68, 2.70 (each s, 2 × 3 H, CH_3, Isomer 2), 6.60 (d, J_{HH} = 7.2 Hz, 2 × 1 H, Ar*H*, Isomers 1 & 2), 6.65 (d, J_{HH} = 7.3 Hz, 2 × 1 H, Ar*H*, Isomers 1 & 2), 6.74 (d, J_{HH} = 7.3 Hz, 1 H, Ar*H*, Isomer 1), 6.87 (d, J_{HH} = 8.0 Hz, 1 H, Ar*H*, Isomer 1), 7.04 (t, J_{HH} = 7.4 Hz, 2 H, Ar*H*, Isomer 2), 7.15 (d, J_{HH} = 8.0 Hz, 2 × 2 H, Ar*H*, Isomers 1 & 2), 7.34 (t, J_{HH} = 8.0 Hz, 2 H, Ar*H*, Isomer 2), 7.45 (t, J_{HH} = 7.7 Hz, 1 H, Ar*H*, Isomer 1), 7.51 (t, J_{HH} = 7.7 Hz, 1 H, Ar*H*, Isomer 1), 7.74 (d, J_{HH} = 8.1 Hz, 2 H, Ar*H*, Isomer 1), 7.87 (d, J_{HH} = 8.4 Hz, 2 H, Ar*H*, Isomer 2), 12.23 (s, 1 H, NH, Isomer 1), 12.35 (s, 1 H, NH, Isomer 2), 14.32 (s, 1 H, NH, Isomer 1) (see Fig. 11). The signal for second NH proton of isomer 2 was not observed. ^{13}C {^{1}H} NMR ($CDCl_3$, 100.5 MHz): δ 21.0, 24.2 (*C*H_3), 109.8, 115.0, 115.9, 118.3, 120.7, 129.3, 131.8, 137.4, 137.9, 138.6, 149.1, 153.2, 153.5, 155.2 (ArCH/Ar*C*), 161.5 (*C*N_3). ESI Mass (HRMS) $[M+H]^+$ Calc. 332.1875, Found 332.1861. Anal. Calc for $C_{20}H_{21}N_5$ (Mw = 331.414): C, 72.48; H, 6.39; N, 21.13. Found: C, 72.28; H, 6.72; N, 21.42.

4.7. *[RN=C(NHR)(NHAr)] (R = 6-Me-2-C_5H_3N, Ar = 4-ClC_6H_4; **6**)*

Guanidine, **6** was prepared from *N*,*N*′-bis(6-methyl pyridin-2-yl) thiourea (258 mg, 1.00 mmol), 4-chloroaniline (140 mg, 1.10 mmol), KOH (140 mg as 70% aq. solution) and nitrobenzene (100 mg) by following the procedure analogous to that outlined for **1**. Yield: 75% (264 mg, 0.75 mmol). Mp: 176 °C. ATR–IR (cm^{-1}): ν (NH) 2916 (br, w); ν (C=N) 1659 (m). ^{1}H NMR ($CDCl_3$, 400 MHz): δ 2.52, 2.54 (each s, 2 × 3 H, CH_3) 6.60 (d, J_{HH} = 7.6 Hz, 1 H, Ar*H*), 6.68 (d, J_{HH} = 6.8 Hz, 1 H, Ar*H*), 6.75 (d, J_{HH} = 6.8 Hz, 2 H, Ar*H*), 6.88 (d, J_{HH} = 7.6 Hz, 1 H, Ar*H*), 7.28 (dd, J_{HH} = 7.0; 2.2 Hz, 2 H, Ar*H*), 7.47, 7.53 (each t, J_{HH} = 7.6 Hz, 2 × 1 H, Ar*H*), 7.82 (d, J_{HH} = 8.4 Hz, 1 H, Ar*H*), 12.42 and 14.34 (each s, 2 × 1 H, N*H*). ^{13}C{^{1}H} NMR ($CDCl_3$, 100.5 MHz): δ 24.2 (*C*H_3), 109.8, 115.4, 116.1, 118.3, 121.5, 126.9, 126.6, 138.0, 138.7, 148.8, 153.1, 153.6, 155.2 (Ar*C*/ArCH), 161.1 (*C*N_3). ESI Mass (HRMS) $[M+H]^+$ Calc. 352.1328, Found 352.1329. Anal. Calc for $C_{19}H_{18}N_5Cl$ (Mw = 351.8): C, 64.86; H, 5.16; N, 19.91. Found: C, 64.78; H, 4.89; N, 19.78.

4.8. *[RN=C(NHR)(NHAr)] (R = 6-Me-2-C_5H_3N, Ar = 4-FC_6H_4; **7**)*

Guanidine, **7** was prepared from *N*,*N*′-bis(6-methyl pyridine-2-yl)thiourea (258 mg, 1.00 mmol), 4-fluoroaniline (122 mg, 1.10 mmol), KOH (140 mg as 70% aq. solution) and nitrobenzene (100 mg) by following the procedure analogous to that outlined for **1**. Yield: 75% (238 mg, 0.75 mmol). Mp: 176 °C. ATR–IR (cm^{-1}): ν (NH) 2918 (br, w); ν (C=N) 1657 (m). ^{1}H NMR ($CDCl_3$, 400 MHz): δ 2.52, 2.54 (each s, 2 × 3 H, CH_3), 6.60 (d, J_{HH} = 7.6 Hz, 1 H, Ar*H*), 6.67 (d, J_{HH} = 6.8 Hz, 1 H, Ar*H*), 6.75, 6.86 (each d, J_{HH} = 7.6 Hz, 2 × 1 H, Ar*H*), 7.03 (t, J_{HH} = 8.8 Hz, 2 H, Ar*H*), 7.46 (t, J_{HH} = 7.6 Hz, 1 H, Ar*H*), 7.52 (t, J_{HH} = 8.0 Hz, 1 H, Ar*H*), 7.79–7.83 (m, 2 H, Ar*H*), 12.31 and 14.34 (each s, 2 × 1 H, N*H*). ^{13}C{^{1}H} NMR ($CDCl_3$, 100.5 MHz): δ 24.2 (*C*H_3), 109.8, 115.2 (d, J_{CF} = 22.0 Hz), 116.0, 118.3, 120.6, 121.9 (d, J_{CF} = 7.6 Hz), 122.4, 128.8, 136.1, 138.0, 138.7, 149.0, 153.2, 153.6, 155.2, 158.4 (d, J_{CF} = 241.5 Hz) (ArCH/Ar*C*), 161.3 (*C*N_3). ^{19}F NMR ($CDCl_3$, 376.31 MHz): δ −121.0. ESI Mass (HRMS) $[M+H]^+$

Table 8
Details pertinent to H−MCRs involving methyl acrylate and various aryl chlorides (see Scheme 7). The reported yields represent isolated yields based on an average of two runs.

Entry	Substrate	Product	Yield (%)
1	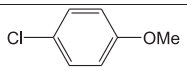	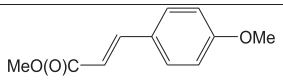	88
2	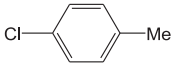	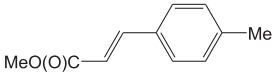	90
3	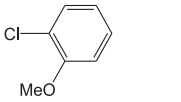	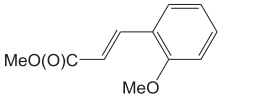	85
4	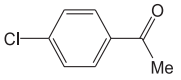	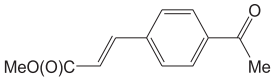	93
5	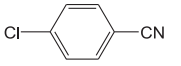	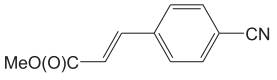	91
6	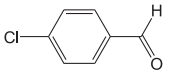	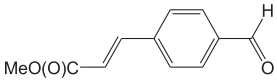	91
7	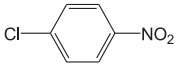	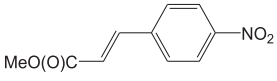	93
8	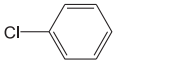	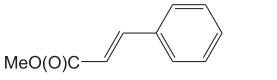	89

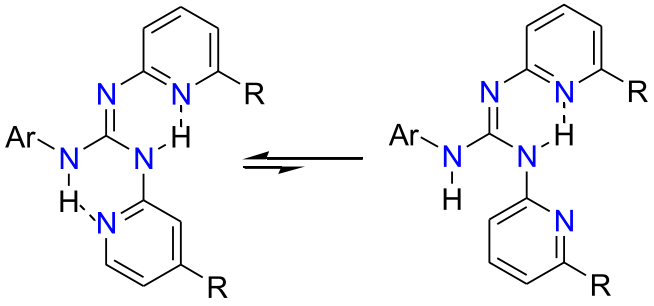

Fig. 11. Possible isomers of guanidines **2** and **5** in solution.

Calc. 336.1624, Found 336.1615. Anal. Calc for $C_{19}H_{18}N_5F$ (Mw = 335.378): C, 68.04; H, 5.41; N, 20.88. Found: C, 68.02; H, 5.65; N, 20.86.

4.9. *[Pd{κ²(N,N)-C_5H_4N-1(N=C(NHAr)(NPy))-2}₂] (Ar = 4-MeC_6H_4; **8**)*

$Pd(OAc)_2$ (50.0 mg, 0.223 mmol), guanidine **2** (135 mg, 0.445 mmol), and toluene (5 mL) were taken in a 25 mL RB flask, fitted with a double surface condenser equipped with a freshly prepared anhyd. $CaCl_2$ guard tube. The mixture was stirred at 60 °C for 3 h to afford **8** as yellow solid. The solid was filtered off, dissolved in CH_2Cl_2, layered with *n*-hexane and stored at room temperature for several days to afford **8** as orange crystals suitable for SCXRD. Yield: 80% (148 mg, 0.18 mmol). Mp: 276 °C. ATR−IR (cm^{-1}): ν (NH) 2934 (br, w); ν (C=N) 1618 (m). ^{1}H NMR ($CDCl_3$, 400 MHz): δ 2.34 (s, 6 H, CH_3), 6.25 (dt, J_{HH} = 6.6; 1.6 Hz, 2 H, Ar*H*), 6.56 (t, J_{HH} = 5.8 Hz, 2 H, Ar*H*), 6.83 (d, J_{HH} = 8.0 Hz, 2 H, Ar*H*), 7.10−7.23 (m, 8 H, Ar*H*), 7.57 (d, J_{HH} = 8.8 Hz, 2 H, Ar*H*), 7.65 (t, J_{HH} = 7.7 Hz, 6 H, Ar*H*), 8.02 (dd, J_{HH} = 4.6; 1.8 Hz, 2 H, Ar*H*), 12.61 (s, 2 H, N*H*). MS (TOF-ES⁺), *m*/*z* (intensity %), $[M+H]^+$ Calc. 711.1924, Found 711.0419. Anal. Calc for $C_{36}H_{32}N_{10}Pd$ (Mw = 711.126): C, 60.80; H, 4.54; N, 19.70. Found: C, 60.60; H, 4.51; N, 19.91.

4.10. *[Pd{κ²(N,N)-C_5H_4N-1(N=C(NHAr)(NPy))-2}₂] (Ar = 4-ClC_6H_4; **9**)*

Complex **9** was prepared from $Pd(OAc)_2$ (50.0 mg, 0.223 mmol) and guanidine **3** (144 mg, 0.445 mmol) in toluene (5 mL) by following the procedure analogous to that outlined for complex **8**. Orange crystals suitable for SCXRD were grown from CH_2Cl_2/cyclohexane mixture over a period of one week at room temperature. Yield: 72% (121 mg, 0.16 mmol). Mp: 263 °C. ATR−IR (cm^{-1}): ν (NH) 2929 (br, w); ν (C=N) 1610 (m). ^{1}H NMR ($CDCl_3$, 400 MHz): δ 6.28, 6.59 (each t, J_{HH} = 6.0 Hz, 2 × 2 H, Ar*H*), 6.85 (d, J_{HH} = 8.4 Hz, 2 H, Ar*H*), 7.15 (dt, J_{HH} = 8.0 Hz; 1.8 Hz, 2 H, Ar*H*), 7.24 (t, J_{HH} = 6.4 Hz, 2 H, Ar*H*), 7.30 (d, J_{HH} = 8.8 Hz, 4 H, Ar*H*), 7.56 (d, J_{HH} = 8.4 Hz, 2 H, Ar*H*), 7.63 (d, J_{HH} = 6.4 Hz, 2 H, Ar*H*), 7.76 (d, J_{HH} = 8.4 Hz, 4 H, Ar*H*), 8.04 (d, J_{HH} = 4.4 Hz, 2 H, Ar*H*), 12.8 (s, 2 H, N*H*). ESI Mass (HRMS) $[M+H]^+$ Calc. 751.0832, Found 751.0819. Anal. Calc for $C_{34}H_{26}N_{10}Cl_2Pd$ (Mw = 751.963): C, 54.31; H, 3.49; N, 18.63. Found: C, 54.00; H, 3.82; N, 18.56.

4.11. [Pd{κ²(N,N)-C_5H_4N-1(N=C(NHAr)(NPy))-2}$_2$] (Ar = 4-BrC_6H_4; **10**)

Complex **10** was prepared from $Pd(OAc)_2$ (50.0 mg, 0.223 mmol) and guanidine **4** (164 mg, 0.445 mmol) in toluene (5 mL) by following the procedure analogous to that outlined for complex **8**. Orange crystals suitable for SCXRD were grown from CH_2Cl_2/cyclohexane mixture over a period of several days at room temperature. Yield: 73% (138 mg, 0.16 mmol). Mp: 261 °C. ATR–IR (cm^{-1}): ν (NH) 2922 (br, w); ν (C=N) 1589 (m). ^1H NMR ($CDCl_3$, 400 MHz): δ 6.28, 6.60 (each t, J_{HH} = 5.8 Hz, 2 × 1 H, Ar*H*), 6.67, 6.71 (each t, J_{HH} = 6.2 Hz, 2 × 1 H, Ar*H*), 6.85, 7.02 (each d, J_{HH} = 8.4 Hz, 2 × 1 H, Ar*H*), 7.15 (dt, J_{HH} = 7.9; 2.0 Hz, 1 H, Ar*H*), 7.23 (d, J_{HH} = 7.2 Hz, 1 H, Ar*H*), 7.37 (d, J_{HH} = 6.4 Hz, 1 H, Ar*H*), 7.43 (t, J_{HH} = 8.8 Hz, 4 H, Ar*H*), 7.48 (d, J_{HH} = 6.0 Hz, 1 H, Ar*H*), 7.51 (t, J_{HH} = 6.6 Hz, 1 H, Ar*H*), 7.56 (d, J_{HH} = 8.4 Hz, 1 H, Ar*H*), 7.61–7.64 (m, 4 H, Ar*H*), 7.72 (d, J_{HH} = 8.8 Hz, 2 H, Ar*H*), 7.94 (d, J_{HH} = 8.4 Hz, 1 H, Ar*H*), 8.04 (d, J_{HH} = 5.2 Hz, 1 H, Ar*H*), 12.26 and 12.80 (each s, 2 × 1 H, N*H*). ESI Mass (HRMS) $[M+H]^+$ Calc. 838.9822, Found 838.9784. Anal. Calc for $C_{34}H_{26}N_{10}Br_2Pd$ (Mw = 840.805): C, 48.56; H, 3.12; N, 16.66. Found: C, 48.80; H, 3.28; N, 16.99.

4.12. [Pd{κ²(N,N)-C_5H_3N-1-Me-6(N=C(NHAr)(N(6-MePy))-2}$_2$] (Ar = 4-MeC_6H_4; **11**)

Complex **11** was prepared from $Pd(OAc)_2$ (50.0 mg, 0.223 mmol) and guanidine **5** (147 mg, 0.445 mmol) in toluene (5 mL) by following the procedure analogous to that outlined for complex **8**. Red crystals suitable for SCXRD were grown from CH_2Cl_2/cyclohexane mixture over a period of several days at room temperature. Yield: 79% (135 mg, 0.18 mmol). Mp: 258 °C (decomp.). ATR–IR (cm^{-1}): ν (NH) 2914 (br, w); ν (C=N) 1618 (m). ^1H NMR ($CDCl_3$, 400 MHz): δ 2.16, 2.19, 2.33 (each s, 6 × 3 H, CH_3), 6.49 (d, J_{HH} = 6.6 Hz, 2 H, Ar*H*), 6.56 (d, J_{HH} = 7.3 Hz, 2 H, Ar*H*), 6.85 (d, J_{HH} = 8.1 Hz, 2 H, Ar*H*), 7.13 (t, J_{HH} = 8.1 Hz, 4 H, Ar*H*), 7.34, 7.46 (each t, J_{HH} = 7.7 Hz, 2 × 2 H, Ar*H*), 7.53 (d, J_{HH} = 8.0 Hz, 4 H, Ar*H*), 7.73 (d, J_{HH} = 8.1 Hz, 2 H, Ar*H*), 12.53 (s, 2 H, N*H*). ESI Mass (HRMS) $[M+H]^+$ Calc. 767.2550, Found 767.2512. Anal. Calc for $C_{40}H_{40}N_{10}Pd$ (Mw = 767.233): C, 62.62; H, 5.25; N, 18.26. Found: C, 62.31; H, 5.24; N, 18.42.

4.13. [Pd{κ²(N,N)-C_5H_3N-1-Me-6(N=C(NHAr)(N(6-MePy))-2}$_2$] (Ar = 4-ClC_6H_4; **12**)

Complex **12** was prepared from $Pd(OAc)_2$ (50.0 mg, 0.223 mmol) and guanidine **6** (156.6 mg, 0.445 mmol) in toluene (5 mL) by following the procedure analogous to that outlined for complex **8**. Red crystals suitable for SCXRD were grown from CH_2Cl_2/cyclohexane mixture over a period of several days at room temperature. Yield: 69% (124 mg, 0.15 mmol). Mp: 270 °C (decomp.). ATR–IR (cm^{-1}): ν (NH) 2922 (w); ν (C=N) 1593 (m). The ^1H NMR spectrum of **12** revealed the presence of three isomers in *ca* 1.00:0.08:0.03 ratio as estimated from the integrals of N*H* protons (see Fig. 12). ^1H NMR ($CDCl_3$, 400 MHz): δ 2.17, 2.20 (each s, 4 × 3 H, CH_3, Isomer 1), 2.41 (s, 2 × 3 H, CH_3, Isomer 2), 2.52, 2.54 (each s, 4 × 3 H, CH_3, Isomer 3), 2.84 (s, 2 × 3 H, CH_3, Isomer 2), 6.14 (d, J_{HH} = 7.2 Hz, 2 H, Ar*H*, Isomer 3), 6.43 (d, J_{HH} = 7.2 Hz, 2 H, Ar*H*, Isomer 2), 6.53 (d, J_{HH} = 7.3 Hz, 2 H, Ar*H*, Isomer 1), 6.58 (d, J_{HH} = 7.3 Hz, 2 × 2 H, Ar*H*, Isomers 1 & 3), 6.71 (d, J_{HH} = 8.8 Hz, 2 H, Ar*H*, Isomer 2), 6.75 (d, J_{HH} = 6.0 Hz, 2 H, Ar*H*, Isomer 2), 6.86 (d, J_{HH} = 8.0 Hz, 2 × 2 H, Ar*H*, Isomers 1 & 3), 7.01 (t, J_{HH} = 7.4 Hz, 2 H, Ar*H*, Isomer 2), 7.07 (d, J_{HH} = 8.0 Hz, 2 H, Ar*H*, Isomer 2), 7.11 (d, J_{HH} = 8.4 Hz, 2 H, Ar*H*, Isomer 2), 7.27 (d, J_{HH} = 8.8 Hz, 3 × 4 H, Ar*H*, Isomers 1, 2 & 3), 7.38 (t, J_{HH} = 7.7 Hz, 3 × 2 H, Ar*H*, Isomers 1, 2 & 3), 7.44 (t, J_{HH} = 7.7 Hz, 2 × 2 H, Ar*H*, Isomers 1 & 3), 7.61 (d, J_{HH} = 8.8 Hz, 2 × 4 H, Ar*H*, Isomers 1 & 3), 7.70 (d, J_{HH} = 8.1 Hz,

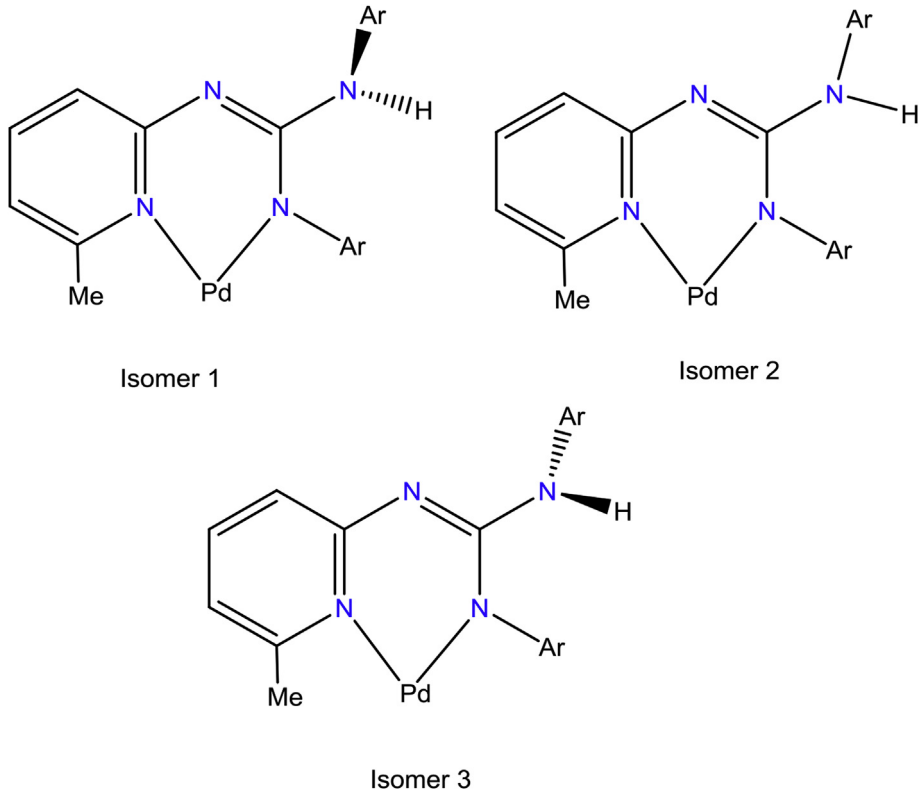

Fig. 12. Possible isomers of **12** and **13** in solution.

2 × 2 H, Ar*H*, Isomers 1 & 3), 7.82 (d, J_{HH} = 8.0 Hz, 2 H, Ar*H*, Isomer 2), 12.59 (s, 2 H, N*H*, Isomer 2), 12.68 (s, 2 H, N*H*, Isomer 1), 13.25 (s, 2 H, N*H*, Isomer 3). Isomers 2 and 3 could possibly arise from the isomer 1 through two independent restricted C–N(H)Ar single bond rotations of the guanidinato ligand [40]. ESI Mass (HRMS) $[M+H]^+$ Calc. 807.1457, Found 807.1394. Anal. Calc for $C_{38}H_{34}N_{10}Cl_2Pd$ (Mw = 808.07): C, 56.48; H, 4.24; N, 17.33. Found: C, 56.72; H, 4.42; N, 17.28.

4.14. [Pd{κ²(N,N)-C₅H₃N-1-Me-6(N=C(NHAr)(N(6-MePy))-2}₂] (Ar = 4-FC₆H₄; **13**)

Complex **13** was prepared from $Pd(OAc)_2$ (50 mg, 0.223 mmol) and guanidine **7** (149.2 mg, 0.445 mmol) in toluene (5 mL) by following the procedure analogues to that outlined for complex **8**. Red crystals suitable for SCXRD were grown from CH_2Cl_2/cyclohexane mixture over a period of several days at room temperature. Yield: 73% (126 mg, 0.16 mmol). Mp: 233 °C (decomp.). ATR–IR (cm^{-1}): *ν* (NH) 2922 (br, w); *ν* (C=N) 1570 (m). The ^1H NMR spectrum of **13** revealed the presence of two isomers in *ca* 1.00:0.36 ratio as estimated from the integrals of N*H* protons (see Fig. 12). ^1H NMR ($CDCl_3$, 400 MHz): *δ* 2.14, 2.18 (each s, 8 × 3 H, C*H*$_3$, Isomers 1 & 2), 6.49 (d, J_{HH} = 6.8 Hz, 2 × 2 H, Ar*H*, Isomers 1 & 2), 6.56 (d, J_{HH} = 7.2 Hz, 2 × 2 H, Ar*H*, Isomers 1 & 2), 6.83 (d, J_{HH} = 8.0 Hz, 2 H, Ar*H*, Isomer 1), 6.87 (d, J_{HH} = 8.4 Hz, 2 H, Ar*H*, Isomer 2), 7.02 (t, J_{HH} = 8.6 Hz, 2 × 4 H, Ar*H*, Isomers 1 & 2), 7.32–7.36 (m, 6H, Ar*H*, 2H (Isomer 1) & 4H (Isomer 2)), 7.45 (t, J_{HH} = 7.6 Hz, 2 × 2 H, Ar*H*, Isomers 1 & 2), 7.58–7.61 (m, 6 H, Ar*H*, Isomer 1 (4 H) & Isomer 2 (2 H)), 7.66 (d, J_{HH} = 8.0 Hz, 2 H, Ar*H*, Isomer 2), 7.72 (d, J_{HH} = 8.0 Hz, 2 H, Ar*H*, Isomer 1), 12.59 (s, 2 H, N*H*, Isomer 1), 12.61 (s, 2 H, N*H*, Isomer 2). $^{13}C\{^1H\}$ NMR ($CDCl_3$, 100.5 MHz): *δ* 23.61, 24.91 (*C*H$_3$), 114.88, 115.26 (d, J_{CF} = 22.1 Hz), 116.61, 116.63 (d, J_{CF} = 22.2 Hz, Isomer 2), 118.52, 121.12, 122.31, 122.53 (d, J_{CF} = 7.6 Hz), 128.78, 136.78, 137.21, 138.07, 140.75, 152.00, 152.09, 152.13, 155.53, 158.49 (d, J_{CF} = 240.8 Hz), 159.51, 159.86 (ArCH/Ar*C*/*C*N$_3$). The isomer 2 could possibly arise from the isomer 1 through a restricted C–N(H)Ar single bond rotation of the guanidinato ligand. ^{19}F NMR ($CDCl_3$, 376.31 MHz): *δ* −121.16. ESI Mass (HRMS) $[M+H]^+$ Calc. 775.2048, Found 775.2078. Anal. Calc for $C_{38}H_{34}N_{10}F_2Pd$ (Mw = 775.16): C, 58.88; H, 4.42; N, 18.07. Found: C, 58.98; H, 4.49; N, 18.32.

4.15. General procedure for H-MCR of aryl bromides with styrene

To a 25 mL RB flask was taken styrene (145.8 mg, 1.4 mmol), aryl bromide (1.0 mmol), sodium acetate (90.2 mg, 1.1 mmol), TBAB (2.0 gm, 6.2 mol) and the catalyst (0.8 mg, 0.001 mmol). The reaction mixture was heated to 120 °C and stirred at the same temperature for 12 h and cooled. The organic portion from the reaction mixture was extracted with diethyl ether (2 × 15 mL). The extracts were combined and the volatiles removed on a rotavapor. The desired coupling product was isolated on a silica gel column using *n*-hexane→ethyl acetate/*n*-hexane (2/98, v/v) mixture as eluent.

4.16. General procedure for H-MCR of aryl chlorides with styrene and methyl acrylate

To a 25 mL RB flask was taken styrene (145.8 mg, 1.4 mmol) or methyl acrylate (120.5 mg, 1.4 mmol), aryl chloride (1.0 mmol), sodium acetate (90.2 mg, 1.1 mmol), TBAB (2.0 gm, 6.2 mol) and the catalyst (4.0 mg, 0.005 mmol). The reaction mixture was heated to 120 °C and stirred at the same temperature for 24 h and cooled. The organic portion from the reaction mixture was extracted with diethyl ether (2 × 15 mL). The extracts were combined and the volatiles removed on a rotavapor. The desired coupling product was isolated on a silica gel column using *n*-hexane→ethyl acetate/*n*-hexane (2/98, v/v) mixture as eluent.

4.17. Neat reaction involving **9** and TBAB

Complex **9** (301 mg, 0.40 mmol) and TBAB (2.0 gm, 6.20 mol) were taken a 25 mL RB flask. The reaction mixture was heated to 120 °C and stirred at the same temperature for 12 h and cooled. Subsequently, the reaction mixture was diluted with chloroform (50 mL) and centrifuged to afford a black palladium powder. The powder was washed with chloroform (2 × 10 mL) and dried in an oven at 70 °C for an hour. Yield: 85% (36 mg, 0.34 mmol).

Acknowledgements

We thank University of Delhi and Department of Science and Technology, New Delhi for DU-DST research grant and one of us (V.M.) acknowledges Council of Scientific and Industrial Research, New Delhi for a fellowship.

Appendix A. Supplementary data

Supplementary data to this article can be found online at https://doi.org/10.1016/j.jorganchem.2019.04.009.

References

[1] (a) P.J. Bailey, S. Pace, The coordination chemistry of guanidines and guanidinates, Coord. Chem. Rev. 214 (2001) 91–141;
(b) P. Bazinet, D. Wood, G.P.A. Yap, D.S. Richeson, Synthesis and structural investigation of *N,N′,N″*-trialkylguanidinato supported zirconium(IV) complexes, Inorg. Chem. 42 (2003) 6225–6229;
(c) M.P. Coles, Application of neutral amidines and guanidines in coordination chemistry, Dalton Trans. (2006) 985–1001;
(d) F.T. Edelmann, Advances in the coordination chemistry of amidinate and guanidinate ligands, Adv. Organomet. Chem. 57 (2008) 183–352.
[2] (a) K.T. Holman, S.D. Robinson, A. Sahajpal, J.W. Steed, *N,N′,N″*-Triphenylguanidinate(1−) complexes of ruthenium and palladium: syntheses and crystal structures, J. Chem. Soc., Dalton Trans. (1999) 15–18;
(b) J.F. Ferry, F.A. Cotton, S.A. Ibragimov, C.A. Murillo, X. Wang, Searching for precursors to metal–metal bonded dipalladium species: a study of Pd_2^{4+} complexes, Inorg. Chem. 44 (2005) 6129–6137.
[3] (a) N. Mincheva, T. Todorov, O. Angelova, P. J. Bailey, M. Mitewa, Synthesis and structure of Pd(II) complexes of 1,2,3-triphenylguanidine, J. Coord. Chem. 50 (2000) 169–176;
(b) I. Georgieva, N. Mintcheva, N. Trendafilova, M. Mitewa, IR study of the N,N′,N″-triphenylguanidine and its imine nitrogen coordinated Pd(II) complexes, Vib. Spectrosc. 27 (2001) 153–164.
[4] I.M. Muller, R. Robson, A new class of easily obtained carbonate related μ_3-ligands and a protein-sized doughnut-shaped coordination oligomer, Angew. Chem. Int. Ed. 39 (2000) 4357–4359.
[5] (a) S. Li, H. Xie, S. Zhang, Y. Lin, J. Xu, J. Cao, Tetramethylguanidine as an inexpensive and efficient ligand for the palladium catalyzed Heck reaction, Synlett (2005) 1885–1888;
(b) S. Li, Y. Lin, H. Xie, S. Zhang, J. Xu, Brønsted guanidine acid–base ionic liquids: novel reaction media for the palladium catalyzed Heck reaction, Org. Lett. 8 (2006) 391–394;
(c) S. Li, Y. Lin, J. Cao, S. Zhang, Guanidine/$Pd(OAc)_2$ catalyzed room temperature Suzuki cross-coupling reaction in aqueous media under aerobic conditions, J. Org. Chem. 72 (2007) 4067–4072.
[6] P. Agarwal, N. Thirupathi, M. Nethaji, Syntheses, structural aspects, solution behavior, and catalytic utility of cyclopalladated N,N′,N″-triarylguanidines [κ²(C,N))Pd(pyrazole)$_2$X] (X = Br, OC(O)CF_3, and PF_6) in Suzuki-Miyaura coupling reactions of aryl bromides, Organometallics 35 (2016) 3112–3123.
[7] P. Elumalai, R. Ujjval, M. Nethaji, N. Thirupathi, Syntheses, characterization, solution behavior and catalytic activity of *trans*-[(guanidine)$_2$PdX$_2$] (X = Cl and OC(O)R; R = Me, Ph and ^{t}Bu) in Heck-Mizoroki coupling reactions involving chloroarenes/methyl acrylate, Polyhedron 151 (2018) 313–322.
[8] A. Grirrane, H. Garcia, E. Alvarez, Isolation and X-ray characterization of palladium-N complexes in the guanylation of aromatic amines. Mechanistic implications, Beilstein J. Org. Chem. 9 (2013) 1455–1462.
[9] K. Gopi, B. Rathi, N. Thirupathi, Synthesis and conformational features of sym N,N′,N″-triarylguanidines, J. Chem. Sci. 122 (2010) 157–167.
[10] P. Molina, E. Aller, A. Lorenzo, One-flask conversion of N-aryliminophosphoranes into N1,N2,N3-triarylguanidines promoted by TBAF, Synlett (2003) 714–716.

[11] A. Hadzovic, D. Song, Syntheses, structures, and reactivities of novel palladium β-diiminato-acetate complexes, Inorg. Chem. 47 (2008) 12010–12017.

[12] S. Aharonovich, M. Kapon, M. Botoshanski, M.S. Eisen, N, N′-Bis-silylated lithium aryl amidinates: Synthesis, characterization, and the gradual transition of coordination mode from σ toward π originated by crystal packing interactions, Organometallics 27 (2008) 1869–1877.

[13] CSD Version 5.38 Updates (Nov 2016) Reference Codes: EFOFIP, EWOKEG, GAGDUP, KELFAJ, MIFSUQ, QOFFIA, SASVUD, TAFNET, EPALUD, FUDTUU (*Trans*). FONYAI (*Cis*).

[14] P. Srinivas, K. Srinivas, P.R. Likhar, B. Sridhar, K.V. Mohan, S. Bhargava, M.L. Kantam, Uridate/pyridyl Pd(II) complexes: phosphine-free high turnover catalysts for the Heck reaction of deactivated aryl bromides, J. Organomet. Chem. 696 (2011) 795–801.

[15] C. Janiak, A critical account on π–π stacking in metal complexes with aromatic nitrogen-containing ligands, J. Chem. Soc., Dalton Trans. (2000) 3885–3896.

[16] A.J. Blake, R.O. Gould, T.I. Hyde, M. Schroder, Tetrahedral distortion in palladium(II) macrocyclic complexes: the single crystal X-ray structure of $[Pd(tbc)](PF_6)_2 \cdot 0.4\ MeNO_2$ (tbc = 1,4,8,11-tetrabenzyl-l,4,8,11-tetra-azacyclotetradecane), J. Chem. Soc., Chem. Commun. (1987) 1730–1732.

[17] (a) I.P. Beletskaya, A.P. Cheprakov, The Heck reaction as a sharpening stone of palladium catalysis, Chem. Rev. 100 (2000) 3009–3066;
(b) K.R. Balinge, P.R. Bhagat, Palladium-N-heterocyclic carbene complexes for the Mizoroki-Heck reaction: an appraisal, C. R. Chimie. 20 (2017) 773–804;
(c) A. Kumbhar, Functionalized nitrogen ligands for palladium catalysed cross-coupling reactions (Part I), J. Organomet. Chem. 848 (2017) 22–88;
(d) S. Jagtap, Heck reaction–State of the art, Catalysts 7 (2017) 267–320.

[18] (a) P. Srinivas, P.R. Likhar, H. Maheshwaran, B. Sridhar, K. Ravikumar, M.L. Kantam, N4-Tetradentate dicarboxyamidate/dipyridyl palladium complexes as robust catalysts for the Heck reaction of deactivated aryl chlorides, Chem. Eur J. 15 (2009) 1578–1581;
(b) S. Layek Anuradha, B. Agrahari, D.D. Pathak, Synthesis and characterization of a new Pd(II) Schiff base complex $[Pd(APD)_2]$: an efficient and recyclable catalyst for Heck-Mizoroki and Suzuki-Miyaura reactions, J. Organomet. Chem. 846 (2017) 105–112;
(c) F. Schroeter, J. Soellner, T. Strassner, Cross-coupling catalysis by an anionic palladium complex, ACS Catal. 7 (2017) 3004–3009.

[19] (a) S.B. Park, H. Alper, Highly efficient, recyclable Pd(II) catalysts with bisimidazole ligands for the Heck reaction in ionic liquids, Org. Lett. 5 (2003) 3209–3212;
(b) J.-C. Xiao, B. Twamley, J.M. Shreeve, An ionic liquid-coordinated palladium complex: a highly efficient and recyclable catalyst for the Heck reaction, Org. Lett. 6 (2004) 3845–3847;
(c) L. Wang, H. Li, P. Li, Task-specific ionic liquid as base, ligand and reaction medium for the palladium-catalyzed Heck reaction, Tetrahedron 65 (2009) 364–368;
(d) C.I.M. Santos, J.F.B. Barata, M.A.F. Faustino, C. Lodeiro, M.G.P.M.S. Neves, Revisiting Heck–Mizoroki reactions in ionic liquids, RSC Adv. 3 (2013) 19219–19238;
(e) F.R. Fortea-Pérez, B.L. Rothenpieler, N. Marino, D. Armentano, G. De Munno, M. Julve, S.-E. Stiriba, Bis(*N*-substituted oxamate)palladate(II) complexes as effective catalysts for sustainable Heck carbon–carbon coupling reactions in n-Bu_4NBr as the solvent, Inorg. Chem. Front. 2 (2015) 1029–1039.

[20] (a) J.G. de Vries, A unifying mechanism for all high-temperature Heck reactions. The role of palladium colloids and anionic species, Dalton Trans. (2006) 421–429;
(b) D. Astruc, Palladium nanoparticles as efficient green homogeneous and heterogeneous carbon–carbon coupling precatalysts: a unifying view, Inorg. Chem. 46 (2007) 1884–1894;
(c) A.M. Trzeciak, J.J. Ziolkowski, Monomolecular, nanosized and heterogenized palladium catalysts for the Heck reaction, Coord. Chem. Rev. 251 (2007) 1281–1293.

[21] A.F. Littke, G.C. Fu, Palladium-catalyzed coupling reactions of aryl chlorides, Angew. Chem. Int. Ed. 41 (2002) 4176–4211.

[22] U. El-Ayaan, Pt(II), Pd(II) and UO_2(II) complexes of N,N′-bis(2-pyridyl)thiourea; Structural, thermal and biological studies, J. Mol. Struct. 998 (2011) 11–19.

[23] ENHANCE, Oxford Xcalibur Single Crystal Diffractometer, Version 1.171.34.49, Oxford Diffraction Ltd, Oxford, U.K., 2006.

[24] CrysAlisPro, Version 1.171.34.49, Oxford Diffraction Ltd, Oxford, U.K., 2011.

[25] G.M. Sheldrick, University of Gottingen, Gottingen, Germany, 2017.

[26] L.J. Farrugia, WinGX Suite for small molecule single-crystal crystallography, J. Appl. Crystallogr. 32 (1999) 837–838.

[27] O.V. Dolomanov, L.J. Bourhis, R.J. Gildea, J.A.K. Howard, H. Puschmann, OLEX2: a complete structure solution, refinement and analysis program, J. Appl. Crystallogr. 42 (2009) 339–341.

[28] A.D. Becke, Density-functional exchange-energy approximation with correct asymptotic behavior, Phys. Rev. A 38 (1988) 3098–3100.

[29] A.D. Becke, A new mixing of Hartree–Fock and local density–functional theories, J. Chem. Phys. 98 (1993) 1372–1377.

[30] A.D. Becke, Density-functional thermochemistry. III. The role of exact exchange, J. Chem. Phys. 98 (1993) 5648–5652.

[31] R. Krishnan, J.S. Binkley, R. Seeger, J.A. Pople, Self-consistent molecular orbital methods. XX. A basis set for correlated wave functions, J. Chem. Phys. 72 (1980) 650–654.

[32] T.H. Dunning Jr., P.J. Hay, in: H.F. Schaefer III (Ed.), Modern Theoretical Chemistry, Plenum, New York, 1976.

[33] P.J. Hay, W.R. Wadt, *Ab initio* effective core potentials for molecular calculations. Potentials for the transition metal atoms Sc to Hg, J. Chem. Phys. 82 (1985) 270–283.

[34] W.R. Wadt, P.J. Hay, *Ab initio* effective core potentials for molecular calculations. Potentials for main group elements Na to Bi, J. Chem. Phys. 82 (1985) 284–298.

[35] P.J. Hay, W.R. Wadt, *Ab initio* effective core potentials for molecular calculations. Potentials for K to Au including the outermost core orbitals, J. Chem. Phys. 82 (1985) 299–310.

[36] E. Cancès, B. Mennucci, J. Tomasi, A new integral equation formalism for the polarizable continuum model: theoretical background and applications to isotropic and anisotropic dielectrics, J. Chem. Phys. 107 (1997) 3032–3041.

[37] M. Cossi, V. Barone, B. Mennucci, J. Tomasi, Ab initio study of ionic solutions by a polarizable continuum dielectric model, Chem. Phys. Lett. 286 (1998) 253–260.

[38] B. Mennucci, J. Tomasi, Continuum solvation models: a new approach to the problem of solute's charge distribution and cavity boundaries, J. Chem. Phys. 106 (1997) 5151–5158.

[39] M.J. Frisch, G.W. Trucks, H.B. Schlegel, G.E. Scuseria, M.A. Robb, J.R. Cheeseman, J.A. Montgomery Jr., T. Vreven, K.N. Kudin, J.C. Burant, J.M. Millam, S.S. Iyengar, J. Tomasi, V. Barone, B. Mennucci, M. Cossi, G. Scalmani, N. Rega, G.A. Petersson, H. Nakatsuji, M. Hada, M. Ehara, K. Toyota, R. Fukuda, J. Hasegawa, M. Ishida, T. Nakajima, Y. Honda, O. Kitao, H. Nakai, M. Klene, X. Li, J.E. Knox, H.P. Hratchian, J.B. Cross, C. Adamo, J. Jaramillo, R. Gomperts, R.E. Stratmann, O. Yazyev, A.J. Austin, R. Cammi, C. Pomelli, J.W. Ochterski, P.Y. Ayala, K. Morokuma, G.A. Voth, P. Salvador, J.J. Dannenberg, V.G. Zakrzewski, S. Dapprich, A.D. Daniels, M.C. Strain, O. Farkas, D.K. Malick, A.D. Rabuck, K. Raghavachari, J.B. Foresman, J.V. Ortiz, Q. Cui, A.G. Baboul, S. Clifford, J. Cioslowski, B.B. Stefanov, G. Liu, A. Liashenko, P. Piskorz, I. Komaromi, R.L. Martin, D.J. Fox, T. Keith, M.A. Al- Laham, C.Y. Peng, A. Nanayakkara, M. Challacombe, P.M.W. Gill, B. Johnson, W. Chen, M.W. Wong, C. Gonzalez, J.A. Pople, Gaussian09, Rev. A.02, Gaussian, Inc., Wallingford CT, 2009.

[40] T. Singh, R. Kishan, M. Nethaji, N. Thirupathi, Synthesis, reactivity studies, structural aspects, and solution behavior of half sandwich ruthenium(II) *N,N′,N″*-triarylguanidinate complexes, Inorg. Chem. 51 (2012) 157–169.